13.14 Geochemistry of Porphyry Deposits

DR Cooke, University of Tasmania, Hobart, TAS, Australia
P Hollings, Lakehead University, Thunder Bay, ON, Canada
JJ Wilkinson, University of Tasmania, Hobart, Tasmania, Australia; Imperial College London, London, UK
RM Tosdal, University of British Columbia, Vancouver, BC, Canada

13.14.1	**Introduction**	357
13.14.2	**Geology, Alteration, and Mineralization**	357
13.14.3	**Tectonic Setting**	360
13.14.4	**Igneous Petrogenesis**	360
13.14.5	**Geochronology**	363
13.14.6	**Lead Isotopes**	364
13.14.7	**Fluid Inclusions**	366
13.14.8	**Conventional Stable Isotopes**	367
13.14.8.1	Oxygen–Deuterium	367
13.14.8.2	Sulfur	367
13.14.8.3	Carbon–Oxygen	370
13.14.9	**Nontraditional Stable Isotopes**	370
13.14.9.1	Copper	370
13.14.9.2	Molybdenum	372
13.14.9.3	Iron	373
13.14.9.4	Summary	373
13.14.10	**Ore-Forming Processes**	373
13.14.11	**Exploration Model**	375
Acknowledgments		376
References		376

13.14.1 Introduction

Porphyry ore deposits are the Earth's major resources of copper, molybdenum, and rhenium (Sillitoe, 2010) and also provide significant amounts of gold, silver, and other metals. Mineralization styles include stockwork veins, hydrothermal breccias, and wall-rock replacements. Porphyry deposits form at depths of approximately 1–6 km below the paleosurface due to magmatic–hydrothermal phenomena associated with the emplacement of intermediate to felsic intrusive complexes (Seedorff et al., 2005). Most porphyry deposits have a spatial, temporal, and genetic association with geodynamic processes at convergent plate margins where hydrous melts are generated in the subarc mantle. These oxidized melts transport metals and volatiles to magma chambers located in the mid to upper crust, where fractional crystallization and volatile exsolution result in porphyry ore formation.

Porphyry deposits are typically classified on the basis of their economic metal endowment (Kesler, 1973). Subtypes include porphyry Cu, Au, Mo, Cu–Mo, Cu–Au, and Cu–Au–Mo. There are also examples of porphyry Sn and porphyry W deposits (Seedorff et al., 2005). Porphyry deposits can also be classified on the basis of the composition of magmatic rocks associated with mineralization. This scheme recognizes three subcategories of calc-alkaline porphyry deposits (low-K, medium-K, and high-K) and two subcategories of alkalic porphyry deposits (silica-saturated and silica-undersaturated; Lang et al., 1995). The alkalic porphyries are exclusively of Cu–Au character, whereas calc-alkaline deposits span the entire spectrum of Cu, Au, and Mo mineralization.

13.14.2 Geology, Alteration, and Mineralization

Porphyry deposits are centered on, or hosted within, multiphase intrusive complexes (**Figures 1** and **2(a)**). The geometries of individual intrusions vary from pipes ('pencil' porphyries) to dikes, stocks, and, in rare cases, plutons. In some cases, individual intrusive phases have distinctive phenocryst abundances, mineralogies, and grain sizes, making them easy to discriminate (e.g., Bingham Canyon; Redmond and Einaudi, 2010; **Figure 2(a)**). In other cases, intrusive contacts are more subtle due to similar compositions and textures of the porphyritic rocks (e.g., Lickfold et al., 2003). Sillitoe (2000) outlined field criteria that can be used to locate subtle intrusive contacts in porphyry complexes: (1) abrupt changes in metal assays; (2) veins in the older intrusion that are truncated at the contact with the younger intrusion; (3) xenoliths of older intrusive phases and/or xenoliths containing veins in the younger intrusive phase; (4) less abundant veins, less intense alteration, and greater textural preservation in the younger intrusion; and (5) narrow chilled margins and/or flow alignment of phenocrysts in the younger intrusion.

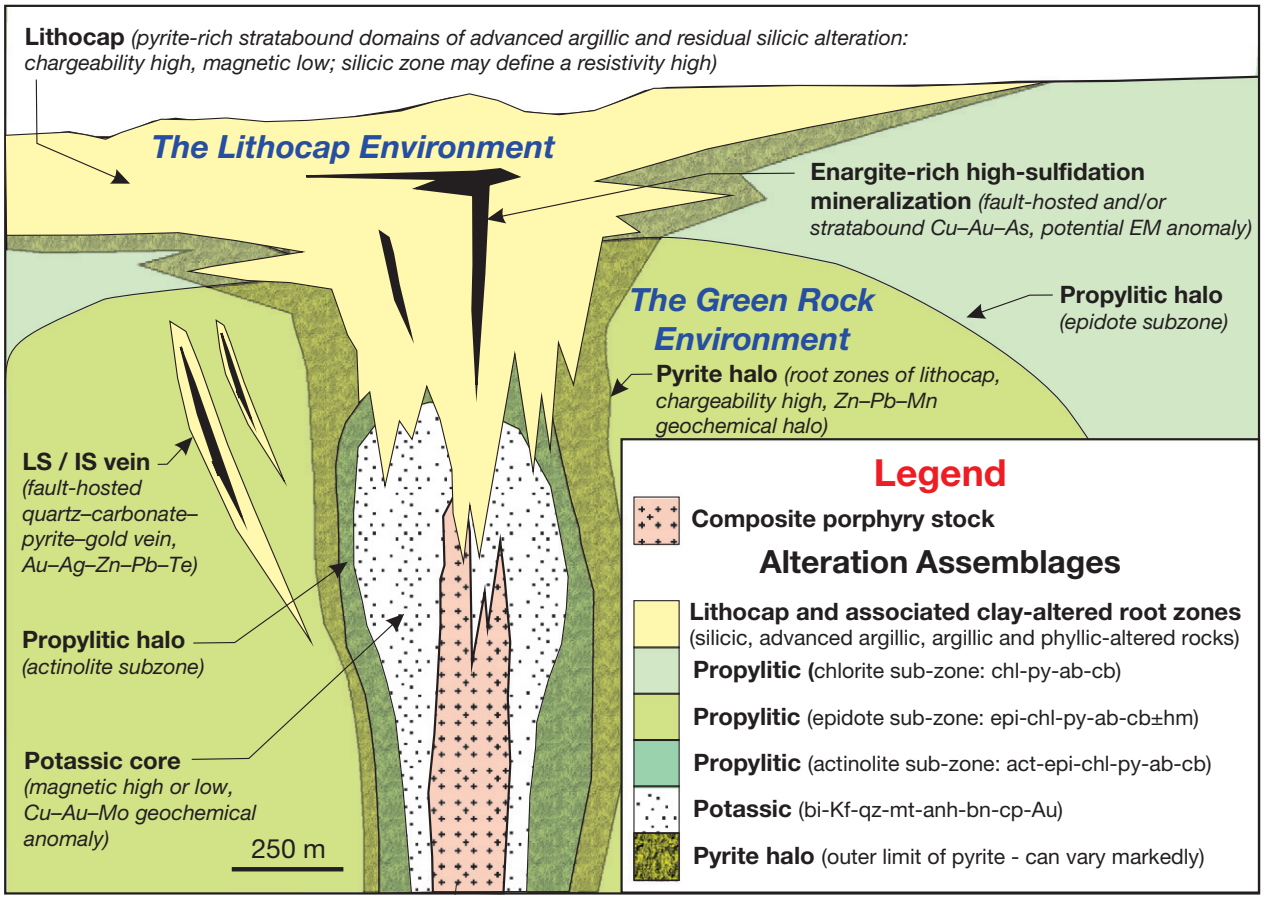

Figure 1 Schematic illustration of alteration zoning and overprinting relationships in a porphyry system (modified after Holliday and Cooke, 2007). Mineralization occurs in potassically altered intrusions and adjacent wall rocks. Three propylitic alteration subfacies (actinolite, epidote, and chlorite zones) can occur around the potassic-altered rocks. In this example, the porphyry has been partially overprinted by a lithocap (silicic and advanced argillic alteration assemblages) that contains a domain of high-sulfidation epithermal mineralization. The roots of the lithocap lie within the pyrite halo to the porphyry system. The degree of superposition of the lithocap into the porphyry system is contingent on uplift and erosion rates at the time of mineralization. *Abbreviations*: ab, albite; act, actinolite; anh, anhydrite; Au, gold; bi, biotite; bn, bornite; cb, carbonate; chl, chlorite; cp, chalcopyrite; epi, epidote; gt, garnet; hm, hematite; Kf, K-feldspar; mt, magnetite; py, pyrite; qz, quartz.

Metal-rich fluids that exsolve from the shallow-crustal intrusive complexes mineralize and alter the upper parts of the causative intrusions and the surrounding country rocks (Burnham, 1979; Henley and McNabb, 1978). Catastrophic fluid release occurs during brittle failure of the magmatic carapace, causing transient depressurization of the intrusive complex (Burnham, 1979). Groundmass crystallization occurs due to pressure quenching, generating the diagnostic porphyritic texture of the mineralizing intrusions. Episodic brittle failure and fluid release from the crystallizing magmas produce a multistage vein stockwork that hosts the bulk of the ore (e.g., Titley, 1982; **Figure 2(b)**). In extreme cases, catastrophic fluid release generates mineralized magmatic–hydrothermal breccia complexes (Burnham, 1985; Sillitoe, 1985; **Figure 2(c)**).

Hydrothermal alteration assemblages define three-dimensional zoning in and around the central, mineralized intrusive complex. A core of potassic alteration forms early in the evolution of the porphyry deposit and is surrounded by a propylitic alteration halo (**Figure 1**). In intermediate to felsic intrusions, the potassic assemblage is dominated by quartz, K-feldspar, anhydrite ± magnetite, chalcopyrite, and bornite. In more mafic wall rocks (e.g., andesite and basalt), the potassic alteration assemblage is dominated by biotite and magnetite, with lesser quartz, K-feldspar, anhydrite, and Cu–Fe sulfides (Meyer and Hemley, 1967; Rose and Burt, 1979; Titley, 1982). These differences are particularly well defined at El Teniente, Chile (Cannell et al., 2005; Vry et al., 2010).

In many porphyry deposits, the central potassic domain hosts the bulk of the ore (e.g., Garwin, 2002; Lowell and Guilbert, 1970; Sillitoe and Gappe, 1984; **Figure 2(b)**). Veins commonly define a radial and/or concentric pattern around central intrusions, particularly when the stocks or pipes have circular to slightly elliptical shapes (e.g., Cannell et al., 2005; Heidrick and Titley, 1982), implying that, at this stage of deposit evolution, the local stress regime around the intrusive complex can control vein orientations. In some cases, regional stress fields predominate, resulting in a strong preferred orientation to the veins (e.g., Chuquicamata, Chile; Lindsay et al., 1995) or even sheeted veins and dike swarms (e.g., Cadia East, Australia; Wilson et al., 2007a).

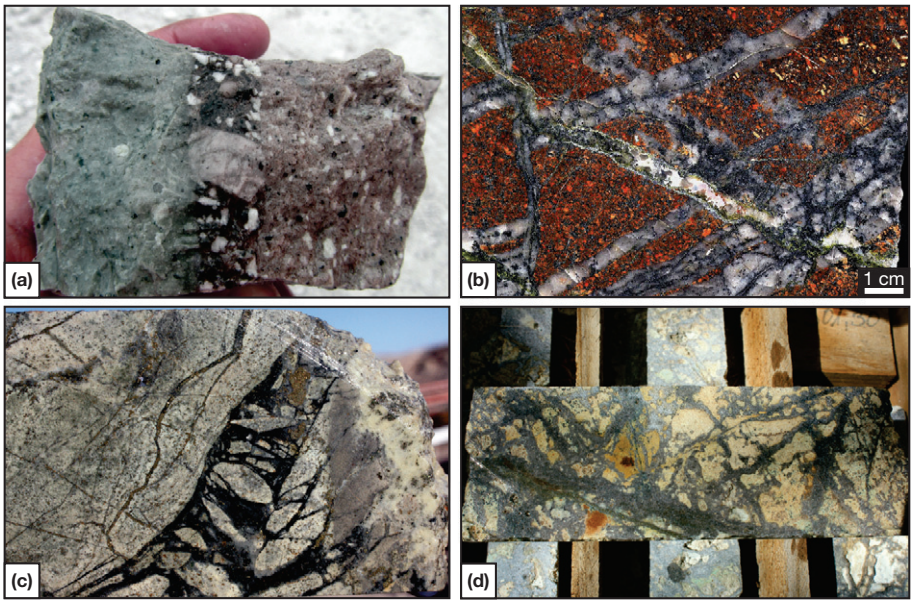

Figure 2 (a) Crosscutting relationships between three intrusive phases from the Bingham Canyon porphyry Cu–Au–Mo deposit, Utah. Individual intrusions have distinctive phenocryst assemblages and textures in this porphyry deposit (e.g., Redmond and Einaudi, 2010). (b) Quartz–magnetite–bornite–gold vein stockwork crosscut by late epidote–calcite–quartz–chalcopyrite vein in orthoclase–actinolite–hematite–altered quartz monzonite, Ridgeway porphyry Au–Cu deposit, NSW. (c) Tourmaline–pyrite–quartz–cemented breccia with quartz–sericite–pyrite alteration halo in granodiorite, Sierra Gorda, Chile. Note the thin quartz–pyrite–tourmaline veinlets that occur as a halo to the tourmaline-cemented breccia. (d) Early porphyry-related quartz vein stockwork overprinted and partly dissolved by late-stage advanced argillic alteration, Caspiche porphyry Au–Cu deposit, Chile.

The propylitic halo extends laterally for kilometers away from the potassic core. It can be divided into three subzones (Holliday and Cooke, 2007): (1) inner, high-temperature actinolite subfacies (actinolite–epidote–chlorite–calcite–pyrite ± magnetite ± hematite ± chalcopyrite); (2) moderate-temperature epidote subfacies (epidote–chlorite–calcite ± pyrite ± hematite ± chalcopyrite); and (3) outer, low-temperature chlorite subfacies (chlorite–calcite ± pyrite ± prehnite ± zeolites; **Figure 1**). Mapping propylitic assemblages can therefore provide a useful vector toward the central, high-temperature mineralized and potassic-altered core of a porphyry deposit.

Late-stage alteration assemblages include phyllic (quartz–muscovite–pyrite ± chalcopyrite), intermediate argillic (illite–chlorite–pyrite–quartz–calcite–hematite ± possibly relict chalcopyrite), argillic (quartz–kaolinite–illite–pyrite), and advanced argillic (quartz–alunite–pyrophyllite–dickite–kaolinite–pyrite ± enargite ± covellite). These clay-rich assemblages are typically localized by faults, are upward-flaring, and overprint the early-formed potassic and propylitic assemblages (**Figures 1** and **2(d)**). Late-stage alteration assemblages are commonly controlled by district-scale faults and subsidiary structures (e.g., Batu Hijau, Indonesia; Garwin, 2002), implying that the regional stress regime controls fluid flow late in the life cycle of a porphyry deposit.

In the near-surface environment (<~1 km below the paleosurface), lateral flow of acidic fluids along permeable horizons may produce thick, extensive domains of clay alteration that are referred to as lithocaps (Chang et al., 2011; Sillitoe, 1995, 2010; **Figure 1**). Lithocaps typically have cores of silicic and advanced argillic alteration surrounded by advanced argillic, argillic, and propylitic alteration assemblages. High-sulfidation state mineralization may occur in the silicic domains (e.g., Cooke and Simmons, 2000). Rapid uplift and erosion during the evolution of a porphyry deposit may cause extreme telescoping, whereby the lithocap overprints the core of the porphyry deposit, producing hybrid high sulfidation – porphyry-style mineralization (e.g., Collahuasi, Chile; Masterman et al., 2005; **Figure 2(d)**). In other cases, where uplift and erosion rates are lower, the lithocap and related high-sulfidation mineralization occur several hundred meters or more above the porphyry deposit (e.g., Lepanto – Far Southeast, Philippines; Chang et al., 2011; Hedenquist et al., 1998).

High-temperature conditions prevail during early vein formation in the core of porphyry deposits, with lower-temperature conditions prevalent during late-stage mineralization. Detailed mapping and logging of the El Salvador porphyry Cu–Mo deposit, Chile, by Anaconda geologists identified a common sequence of vein types that reflects the thermal evolution of magmatic–hydrothermal ore deposits (Gustafson and Hunt, 1975). Early, irregular, discontinuous quartz veins that lack internal symmetry have granular, anhedral mineral textures, and high-temperature alteration assemblages are commonly referred to as 'A-veins.' Straight-sided quartz veins that have more abundant euhedral textures, internal symmetry, central seams of sulfides (e.g., molybdenite and chalcopyrite), and thin halos of potassic alteration are commonly referred to as 'B-veins'; these typically cut A-veins. 'D-veins' are late-stage massive sulfide veins (pyrite ± chalcopyrite ± enargite ± other sulfides, sulfosalts, quartz, and carbonates) that typically have phyllic alteration halos; these crosscut A- and B-veins (Gustafson and Hunt, 1975). Additional vein types have been recognized by other workers. Harris et al. (2003) defined 'P-veins,' early primitive quartz veins that contain melt

inclusions in addition to fluid inclusions. Arancibia and Clark (1996) documented early 'M-veins' at Island Copper (British Columbia). M-veins comprise discontinuous 'chains' or 'beads,' irregular veinlets, and isolated clots of magnetite ± biotite, anhydrite, and Cu–Fe sulfides that commonly predate A-veins. M-veins are now recognized widely as early-formed veins in many other deposits (e.g., Ridgeway, Wilson et al., 2003; El Teniente, Cannell et al., 2005; Vry et al., 2010). Masterman et al. (2005) highlighted late-stage 'E-veins' (enargite-rich veins) that crosscut D-veins at Collahuasi, Chile. **Chapter 13.4** discusses absolute dating of these vein sequences.

13.14.3 Tectonic Setting

Porphyry Cu–Au–Mo deposits are mostly found in continental and oceanic arcs of Tertiary and Quaternary age, notably around the Pacific Rim, but they have also been discovered in ancient fold belts and postcollisional settings (Cooke et al., 2005; Richards, 2009; Sillitoe, 2002). Gold-rich porphyry copper deposits mostly occur in island arc terranes, where emplacement takes place either during or immediately following subduction (Sillitoe, 2002). Some alkalic porphyry copper–gold deposits have formed in anorogenic and extensional intraplate settings (e.g., Richards, 2009). Mineralized alkaline igneous centers also occur in back-arcs, extensional settings, and postsubduction collisional environments (e.g., Hollings et al., 2011a; Wolfe and Cooke, 2011). Most of the fundamental geological characteristics of porphyry systems associated with alkaline rocks are essentially the same as those of deposits accompanying calc-alkaline magmatism (Sillitoe, 2002), except for the alteration assemblages, which include an abundance of Ca-bearing minerals, such as garnet, actinolite, diopside, calcite, and epidote, and the lack of quartz veins and alteration in the silica-undersaturated subtype (Lang et al., 1995).

The recent recognition of porphyry-style mineralization in parts of Tibet, China, and SE Iran that are not connected with active subduction requires an alternative geodynamic model for the formation of some porphyry deposits (Haschke et al., 2010; Hou et al., 2009; Richards, 2009, 2011a,b). In Iran, porphyry-type copper deposits, including Sar Cheshmeh, occur in collisional unroofed Miocene intrusions (Zarasvandi et al., 2005). It is possible that these magmas may be partial remelts of in situ orogenic lower arc crust (Ahmadian et al., 2009; Richards, 2011a; Shafiei et al., 2009) or remelting of previously subducted, modified, metasomatized mantle lithosphere of former arc systems (Haschke et al., 2010).

Although porphyry deposits are typically associated with subduction zones, it has long been recognized that tectonic change is important for porphyry ore genesis. Solomon (1990), Sillitoe (1997), Kerrich et al. (2000), Hollings et al. (2005, 2011b), and others have highlighted the importance of tectonic change for porphyry ore formation. Camus (2003) and Loucks (2012), among others, have noted that in porphyry deposits of Neogene age or younger, mineralization was preceded by, and overlapped with, a 5–10 My episode of uplift and crustal shortening. These episodic events punctuate the steady-state subduction and can be triggered by a variety of causes. Cooke et al. (2005) showed that many giant copper- and gold-rich porphyry deposits are known or inferred to be associated with regions where low-angle subduction of aseismic ridges, seamount chains, or oceanic plateaus was synchronous with ore formation (e.g., **Figure 3**). These 'small' collisions do not cause a cessation of subduction but do result in crustal thickening, rapid uplift, and exhumation. Continental collisions are another, much larger, source of horizontal compression that may cause cessation of subduction. Loucks (2012) suggested that the oblique collision of the Arabian plate with Eurasia during the Paleogene was linked to the formation of Tethyan belt porphyry deposits such as Sungun and the Sar Chesmeh deposit in Iran. The exact relationship between the subduction of aseismic ridges and other upper-plate features with porphyry mineralization remains unclear, but it has been suggested that buoying of the subducting slab creates environments that are favorable for porphyry ore formation (Cooke et al., 2005; **Figure 3**).

The temporal and spatial conjunction of slab flattening with large porphyry deposits has prompted metallogenic modeling directly linking large-scale geodynamic processes with Cu and Au mineralization. Skewes and Stern (1994, 1995, 1996) and Kay and Kurtz (1995) addressed the tectonic and petrochemical environment of the giant Mio–Pliocene porphyry Cu–Mo deposits of Chile. They proposed that progressive slab flattening through the Miocene caused gradual thickening of the subarc continental crust and a concomitant depression of the locus of crustal anatexis. Similarly, Fiorentini and Garwin (2010) have argued that subduction of the buoyant Roo Rise oceanic plateau, south of Sumbawa, Indonesia, caused a kink or tear, in the downgoing slab, which permitted the delivery of mantle-derived melts to the overlying arc and formation of the Batu Hijau deposit (Garwin, 2002). The melts, characterized by a distinctively juvenile radiogenic signature, ascended to upper-crustal levels and underwent fractionation with minimal interaction with the metasomatized lithospheric mantle wedge. Primary hydrous magmatic amphibole grains from the andesite and tonalite intrusions contain extremely low B and Li concentrations, which were interpreted to indicate that the mantle source from which the melts originated was at least partially fluxed by fluids that were not entirely sourced from the dehydration of a subducting slab (Fiorentini and Garwin, 2010). Slab tears have been linked to porphyry ore formation in other regions. At Bajo de la Alumbrera, Argentina, Harris et al. (2004, 2006) argued that a slab tear resulted in asthenospheric mantle welling across the tear to generate fertile mantle. Waters et al. (2011) argued for a slab tear triggering porphyry and epithermal mineralization at the site of ridge subduction in northern Luzon, Philippines (**Figure 3**).

13.14.4 Igneous Petrogenesis

The magmas that crystallize at several kilometers depth in the crust to generate porphyry ore bodies have their origins in the subarc mantle. Melt generation in this region is linked to dehydration and/or melting of the subducting oceanic crust and its veneer of sediment (Best and Christiansen, 2001) and melting of the overlying mantle wedge triggered by the infiltration of slab-derived fluids. The nature of these fluids and

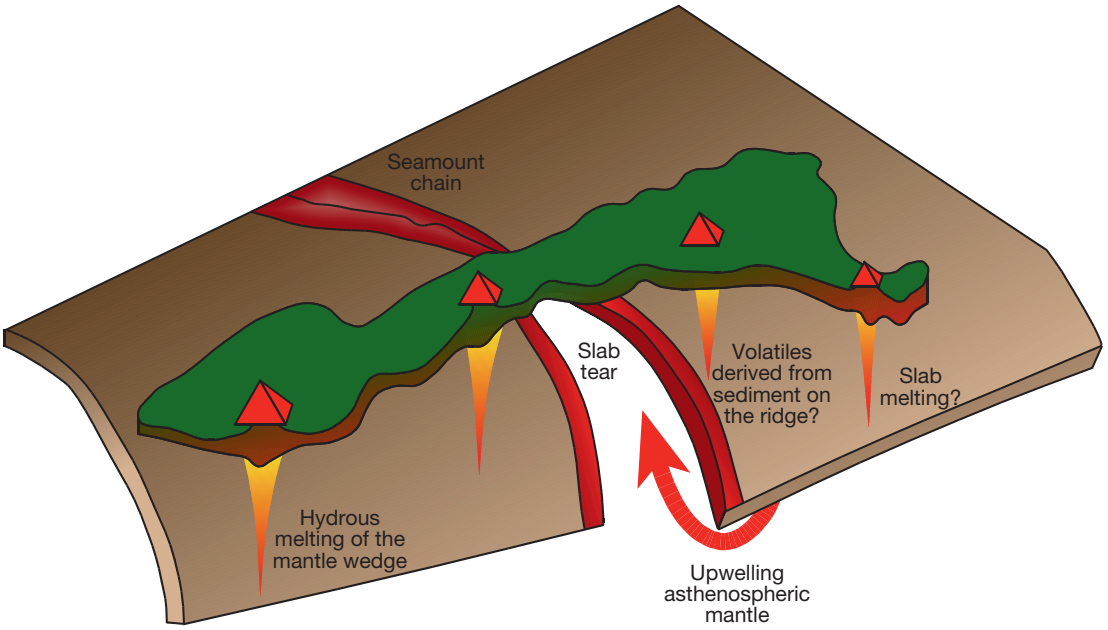

Figure 3 Schematic diagram showing the effects of ridge subduction on the generation of melts in a subduction zone. The model is based on the inferred crustal architecture associated with subduction of the Scarborough Ridge beneath northern Luzon, Philippines, based on data from Yang et al. (1996) and the interpretation of Waters (unpublished data). This ridge subduction event triggered porphyry and epithermal ore formation in the Baguio and Mankayan districts of northern Luzon, resulting in the accumulation of more than 70 Moz Au and 11 Mt Cu in the two districts (Chang et al., 2011; Cooke et al., 2005, 2011; Hollings et al., 2011a,b; Waters et al., 2011). Tearing and flattening of the downgoing slab under such conditions can create conditions that permit slab melting and the formation of oxidized melts conducive to porphyry mineralization.

how they may vary with depth are still a matter of debate (Manning, 2004). Conventionally, it is believed that dehydration of the slab (by breakdown of hydrous minerals) is a principal mechanism for transfer of water-soluble components into the wedge in the shallower parts, whereas melting of the slab sediment, and the basaltic crust itself, may be increasingly important behind the volcanic front (Dreyer et al., 2010; Leeman, 1996). The melts generated in subduction zones are generally high-alumina, hydrous basalt. Interaction of these melts with the continental crust produces the more silica-rich, typically andesitic to dacitic, magmas that form porphyry deposits and build arc volcanoes. This is thought to occur primarily in zones of the lower crust where underplating and/or intrusion of the basaltic melts takes place. In these zones, melting, assimilation, storage, and homogenization (MASH) of lower-crustal rocks and differentiation of the magmas by fractional crystallization produce more silica-rich compositions (Annen et al., 2006; DePaolo, 1981; Hildreth and Moorbath, 1988).

Magmas that source porphyry intrusions are thought to be derived from crustal magma chambers located at 4–10 km depth where, subject primarily to initial water content, andesitic magmas are likely to stall (Annen et al., 2006). These chambers (which ultimately crystallize to intermediate to felsic plutons) grow by the input of magma from the deep-crustal melt generation zone. The minimum size of these chambers can be inferred from estimates of the magma volume required to form giant porphyry deposits (containing >2 Mt Cu; Singer, 1995), which range from 20 to 90 km^3 (Cline and Bodnar, 1991) to >300 km^3 (Cathles and Shannon, 2007). Chambers of this size range are also inferred from studies of modern volcanic eruptions (e.g., Bacon, 1983; Wilson and Hildreth, 1997). Life spans of the associated overlying porphyry and/or volcanic systems of up to 5 My (Sillitoe, 2010) suggest that chambers can remain active for several million years, which are not possible without thermal rejuvenation as a result of the introduction of new magma to the chamber. Consequently, intrusion of multiple batches of andesitic and/or more mafic magma must occur (Glazner et al., 2004). Coupled with open-system convection and a complex range of differentiation processes, new magma injections will modify the magma within the chamber. Episodically, cylindrical intrusions and dike swarms are emplaced upward from the top of the magma chamber and rise to depths of 1–4 km, and it is here that porphyry-related mineralization develops. It is plausible that these events are triggered by hotter mafic intrusions into the chamber (e.g., Sparks and Marshall, 1986), which could cause volatile saturation and the rise of plumes of low-density, bubble-rich magma – the perfect scenario for porphyry ore formation.

Most porphyry deposits are genetically related to intermediate to felsic calc-alkaline magmas (Richards, 2009). The formation of the various styles of porphyry mineralization is connected to the petrogenesis of arc magmas and to the processes of subduction that influence their characteristics (e.g., high oxidation state and enrichment in alkali elements, S, Cl, H_2O, and some metals). With respect to porphyry magma generation, the most important transfers from the subducting slab to the mantle are thought to be those of oxidizing components such as H_2O, CO_2, and possibly ferric iron (Mungall, 2002). Other mobile elements are the large ion lithophile

(Sr and Pb) and high-field-strength elements (U and Th; Massonne, 1992), the tracers of slab sediment input (B and Be; Dreyer et al., 2010; Leeman, 1996) and possibly chlorine (Gill, 1981) and sulfur (Alt et al., 1993). However, the nature of the link between magmatism and the style of mineralization is subject to considerable debate. It has been shown that there are recognizable changes in the geochemistry of the volcanic rocks prior to mineralizing events in northern and central Chile, particularly in terms of the HREE systematics (e.g., Hollings et al., 2005; Kay et al., 1999; Skewes and Stern, 1995; **Figure 3**). Elevated HREE ratios in igneous rocks prior to mineralization have been interpreted either to be the result of gradual crustal thickening of the magmatic arc (Kay et al., 1999) or to be the result of a rapid change in the tectonic environment, probably associated with the subduction of an aseismic ridge (Haschke et al., 2002; Hollings et al., 2005; **Figure 3**). Hollings et al. (2011b) demonstrated the presence of similar trends in the rocks of the Baguio district, Philippines, which formed in association with the subduction of the Scarborough Ridge (Waters et al., 2011). The trends are, however, more subdued, probably as a result of thinner crust in oceanic arc crust.

Numerous authors have argued for a link between adakitic magmas and porphyry mineralization in island arc terranes (Defant and Kepezhinskas, 2001; Hollings et al., 2011a; Polve et al., 2007; Reich et al., 2003; Sajona and Maury, 1998; Thiéblemont et al., 1997) and in intraplate or postsubduction settings unrelated to active subduction (Wang et al., 2007). Although adakites in modern arcs are widely accepted to be the product of slab melts (Defant and Kepezhinskas, 2001), Richards and Kerrich (2007) have suggested that slab melts are commonly misidentified in many geological terranes. More recently, Richards (2011b) has argued that magmas with adakitic Sr/Y and La/Yb characteristics can form at deep-crustal levels because when magmatic water contents are high (e.g., >4 wt% H_2O), then fractionation of amphibole (±garnet) can occur at the same time that plagioclase crystallization is suppressed. Furthermore, Richards (2011a) suggested that although partial melting of the subducted oceanic crust and/or sediments may take place under some conditions, it is not thought to be widespread in modern arcs. Similarly, it is not thought likely that the slab contributes significant chalcophile ore metals based on osmium isotope data (McInnes et al., 1999).

Loucks (2012) suggested that andesites and dacites that are interpreted to be the source of hydrothermal fluids parental to Cu (± Au ± Mo) deposits are characterized by lower Zr, Y, and Yb but higher Sr and Eu values and higher Sr/Zr, Sr/Y, and Eu/Yb ratios than arc magmas unrelated to mineralization. He argued that the porphyry-related magmas could be formed by magmatic differentiation of a hydrous, tholeiitic basaltic parent magma at pressures of 6–13 kbar in chambers that experienced intermittent replenishment by a primitive basaltic melt, broadly similar conditions to those advocated by Richards (2011a). Hornblende crystallization and subsequent suppression of plagioclase and magnetite in long-lived, episodically replenished lower-crustal magma chambers can account for the geochemical characteristics of fertile magmas (Loucks, 2012).

Even though all adakite-like melts may not represent slab melts, their spatial association with porphyry-style mineralization is well documented. Sajona and Maury (1998) speculated on the link between adakites and porphyry deposits. It may be that the generation of adakitic magmas as slab melts is more favorable for the extraction of Au and Cu than slab dehydration. Alternatively, the viscous nature of the adakitic magmas might make them susceptible to crustal entrapment, leading to volatile exsolution and mineralization in the upper crust. Mungall (2002) proposed that silicate melts derived from slab melting have a carrying capacity for Fe_2O_3 some 400 times greater than aqueous fluids. The fluxing of this Fe_2O_3-rich melt through the subarc mantle can lead to the generation of sulfide-undersaturated melting of fertile asthenosphere and the generation of Au- and Cu-rich magmas. It has been postulated that around 25% partial melting of 'normal' mantle would be required to extract all the sulfides present (Barnes and Maier, 1999), although less (~6%) melting may be required if the mantle has been oxidized (Jugo, 2009). Typical arc magmas produced by hydrous fluxing of the asthenospheric mantle wedge will, however, be sulfide-saturated and have low Au and Cu contents (Mungall, 2002). In addition, volatiles derived from sediments on a subducting ridge may cause local metasomatism of the overlying mantle wedge (**Figure 3**). This leads to the generation of oxidized melts that can transport copper, gold, and sulfur dioxide from the mantle to the upper crust (e.g., Mungall, 2002; Richards, 2003; **Figure 3**) and possibly will also provide an additional source of metals. Richards (2011a) suggested that this model may work for Au-rich ore deposits that formed above atypical subduction zones, such as porphyry and epithermal deposits of Papua New Guinea (e.g., Panguna, Ok Tedi, Porgera, and Ladolam) where the ore bodies were generated after reversal of subduction direction led to stalling or tearing of the downgoing slab (Cloos et al., 2005; Mungall, 2002; Solomon, 1990). Richards (2011a) argued that such processes do not, however, account for the formation of most porphyry Cu deposits. In central Chile, Bissig et al. (2003) have argued that slab flattening resulted in the elimination of the subarc asthenospheric mantle and much of the lithospheric mantle in the Miocene beneath the El Indio–Pascua Au–Ag–Cu belt. They argue that this allowed the direct incursion of slab-derived, highly oxidized metal- and volatile-rich supercritical fluids into the lower crust, stimulating melting of mafic, garnet amphibolitic, and eclogitic assemblages and generating the late Miocene metallogenic episode.

Several authors have highlighted the strong association between alkalic magmatism and Au-rich porphyry systems such as Cadia (Holliday et al., 2002), Dinkidi (Hollings et al., 2011a; Wolfe and Cooke, 2011), Northparkes (Heithersay and Walshe, 1995; Lickfold et al., 2007; Müller and Groves, 2000; Müller et al., 1994), and numerous deposits in British Columbia (e.g., Galore Creek, Mt Milligan, Mt Polley, Afton, Ajax, Lorraine; Lang et al., 1995). Sillitoe (2002) noted that mineralization related to alkaline magmatism in arc terranes comprises an unusually large share of the world's giant gold deposits when the small volume of alkaline relative to calc-alkaline rocks is taken into account.

The potential role in porphyry ore formation of oxidized alkalic mafic melts was discussed by Keith et al. (1997). They argued that mafic alkalic melts impacting on the base of the crust, or possibly underplating and being injected into a

mid- to upper-crustal felsic magma chamber, could have a number of consequences. The provision of heat could induce an overturn in the magma chamber and transport volatile-rich magmas to the top of the chamber. Alternatively, the quenching of mafic magma during underplating of the cooler felsic magma chamber could possibly create a stream of volatile and metal-rich magma and bubbles (Keith et al., 1997). Either of these processes could generate magmas that are capable of forming porphyry deposits. Such models have been invoked for the Bingham porphyry (Hattori and Keith, 2001) and the Northparkes Cu–Au deposits of New South Wales (Lickfold et al., 2007).

The presence of porphyry-style mineralization and both alkalic and adakitic rocks in postcollisional, nonarc settings requires some reevaluation of the typical porphyry model. The characteristic mineralization style in extensional postsubduction environments is alkalic-type epithermal Au, associated with mafic alkalic intrusive complexes (Richards, 1995). Examples include Porgera and Ladolam, Papua New Guinea (Müller et al., 2002; Richards et al., 1990); Cripple Creek, Colorado (Jensen and Barton, 2000); and Emperor, Fiji (Eaton and Setterfield, 1993), as well as porphyry Cu mineralization in southeastern Iran (Shafiei et al., 2009). Richards (2009) argued that alkalic epithermal gold deposits form as a result of melting of subduction-modified lithosphere at the base of thickened crust. Davidson et al. (2007) proposed that these amphibole-rich cumulates act like a sponge, storing as much as 20% of the water in the original arc magma. When subjected to a change in the thermal state as a result of overthickening or extension, these amphibolites melt to form magmas with adakitic characteristics. Richards (2009) proposed that, because of the transience of these events compared with steady-state subduction, the magmas will be formed in relatively small volumes and at relatively low degrees of partial melting resulting in magmas that are mildly to strongly alkaline in character (Davies and von Blankenburg, 1995; Jiang et al., 2006).

Based on the Pb isotope characteristics of fluid inclusions from the Bingham porphyry system, Petke et al. (2010) argued that magmas originating from a metasomatized subcontinental lithospheric mantle are the decisive ingredient for the formation of giant Mo-rich porphyry deposits and also for this unique molybdenum ore province, which includes four of the six largest molybdenum deposits in the world (Henderson, Climax, Bingham Canyon, and Butte). They argue that this genetic model for Mo-rich porphyry deposits may also apply to the Gangdese belt in the Tibetan orogen where world-class porphyry Cu–Mo deposits formed from high-K calc-alkaline magmatism some 50 My after arc magmatism (Hou and Cook, 2009).

13.14.5 Geochronology

Porphyry Cu deposits, being products of complex magmatic activity and hydrothermal events in convergent and collisional plate margin (Richards, 2011a; Seedorff et al., 2005; Sillitoe, 2010), require the application of a complete range of geochronologic methods in order to thoroughly understand their evolution and their role within the development of an orogen. It is well documented that porphyry deposits form during narrow time intervals in the life of a magmatic arc and that these belts of porphyry Cu deposits are geographically restricted along the length of the orogen (Sillitoe, 1988). This temporal provinciality is well documented in major porphyry Cu provinces such as the SW United States and adjacent Mexico (Barra et al., 2005), the Andean cordillera (Camus, 2003), the Lachlan orogen of southeast Australia (Glen et al., 2007, 2012), and the Tethyan orogen of eastern Europe to Pakistan (Kouzmanov et al., 2009; Perello et al., 2003; von Quadt et al., 2002; Zimmerman et al., 2008). Within these belts, porphyry Cu systems appear to form during short time intervals. In the Central Andes, these intervals appear to be approximately 10 My as shown by the Paleocene to Eocene belt (62–52 Ma), Eocene to Oligocene belt (42–32 Ma), and Miocene to Pliocene belts (10–4 Ma) of southern Peru and Chile. Similar intervals are recorded in the Lachlan fold belt of Australia (Glen et al., 2007, 2012) and North America (Barra et al., 2005).

Within individual porphyry Cu districts or deposits, U–Pb geochronology on zircon and Ar geochronology on K-bearing minerals, usually biotite and hornblende, have shown magmatic events that occurred over a range of time intervals, varying from 1 My (e.g., Yerington; Dilles and Wright, 1988) to episodic magmatism over 4 My (Sillitoe and Mortensen, 2010). However, not all of the intrusive events contain a porphyry-style hydrothermal system or are equally mineralized (Gustafson et al., 2001; Kouzmanov et al., 2009).

Precise U–Pb geochronology on zircons from multiple porphyry intrusions that form an individual deposit, coupled in some systems with Re–Os ages on molybdenite from the sulfide assemblages (see **Chapter 13.4**), can give conflicting impressions of the duration of an individual porphyry ore-forming event. Short time frames, on the order of a hundred thousand years, have been argued for individual deposits such as Batu Hijau (Garwin, 2002), Bajo de la Alumbrera (von Quadt et al., 2011), Elatsite (von Quadt et al., 2002), Bingham (von Quadt et al., 2011), and Boyongan–Bayugo (Braxton et al., 2012). In contrast, some porphyry Cu deposits are considered to have formed in association with porphyry intrusions emplaced episodically over as much as 4 My, such as at Quellaveco (Sillitoe and Mortensen, 2010), Rio Blanco (Deckart et al., 2005), El Teniente (Maksaev et al., 2004), La Escondida (Padilla-Garza et al., 2004), Chuquicamata (Ballard et al., 2001), Collahuasi (Masterman et al., 2004), and several others. Distinct time gaps, separated by about 1 My (Sillitoe and Mortensen, 2010), and changes in the hydrothermal system characterize these latter deposits. They contain several temporally distinct porphyry complexes, and each may produce an associated hydrothermal system, some of which become weaker with age, whereas others are characterized by distinct hydrothermal alteration styles and associated sulfide minerals. The latter systems are commonly telescoped, with advanced argillic alteration and associated high-sulfidation state minerals, such as those that characterize Chuquicamata (Ossandon et al., 2001), Collahuasi (Masterman et al., 2005), and La Escondida (Padilla-Garza et al., 2004).

Other districts have spatially distinct porphyry Cu centers that may have formed over time. El Salvador has four spatially and temporally distinct porphyry-type hydrothermal centers that formed over 4 My (Cornejo et al., 1997; Gustafson

et al., 2001), the Cadia district has four porphyry centers developed over several million years (Wilson et al., 2007b), whereas Butte has three distinct hydrothermal centers formed over at least 3 My. The youngest hydrothermal center at Butte, the gray sericite zone lying between the Anaconda and Pittsmont porphyry Cu–Mo deposits, is dominated by intense hydrolytic alteration and is spatially associated with, and may even be genetically associated with, the zoned main-stage veins that cut the oldest porphyry Cu center in the Anaconda Dome (Dilles et al., 2003; Rusk et al., 2008). The main-stage veins resulted from the telescoping of a shallower hydrothermal system on top of a deeper porphyry Cu system (Rusk et al., 2008) at a distinctly younger time. Thus, it seems likely that individual porphyry hydrothermal events may be short-lived as suggested in some deposits but where superposed in the same location will constitute a much longer hydrothermal event composed of superposed and temporally distinct systems. It is no surprise that some of the largest porphyry Cu deposits in the world are characterized by repeated cycles of intrusions and mineralization (e.g., Bingham Canyon: Redmond et al., 2004; El Teniente: Cannell et al., 2005; Vry et al., 2010).

Porphyry districts formed over time, either as a single center or as multiple centers, will significantly perturb the thermal structure of the surrounding crust. This occurs largely due to thermally driven convective circulation of groundwater in the propylitic alteration domain and, to a lesser degree, due to conductive heat loss from the large plutonic complex lying at depth (Dilles et al., 2000). The effect of the increased heat will perturb and inhibit rapid cooling of the system, leading to the dominance of minimum K–Ar and ^{40}Ar–^{39}Ar ages of minerals such as biotite, muscovite, and K-feldspar that are characterized by retention temperatures of 350 °C or less (Campos et al., 2009; Harris et al., 2008; Richards et al., 2001). Depending on the depth of formation, the thermal effects can be short-lived or persist for millions of years (Braxton et al., 2012; McInnes et al., 1999).

13.14.6 Lead Isotopes

Radiogenic isotopes, including U–Pb, Sm–Nd, Rb–Sr, and more recently Lu–Hf isotopes, are used extensively to investigate the igneous and hydrothermal evolution of porphyry deposits and the potential sources of contained metals. The U–Pb isotopic system is perhaps the most widely used in studies of porphyry deposits, both as a geochronologic tool and as an isotopic tracer to evaluate magma and metal sources and magma interactions with various reservoirs. This is possible because Pb is a commonly occurring trace or major element in many rock-forming silicate minerals and also in many of the sulfide minerals that occur in porphyry deposits. Although many studies compare Pb isotopic compositions in porphyry Cu-related rocks and hydrothermal minerals to model reservoirs (e.g., Stacey and Kramers, 1975; Zartman and Doe, 1981), magmatic and hydrothermal processes can be better constrained by placing those isotopic data within the ranges of Pb isotopic reservoirs potentially present in the area under investigation or establishing a Pb isotopic evolution history that is unique to a particular region (e.g., Arribas and Tosdal, 1994; Carr et al., 1995).

Two related aspects of Pb isotopes are important to tracking metal sources and understanding the magmatic and ore-forming processes. First, there are large-scale crustal domains characterized by distinct isotopic evolution histories controlled by their Th/U and U/Pb ratios (e.g., Chiaradia and Fontbote, 2002; Kamenov et al., 2002; MacFarlane et al., 1990; Wooden et al., 1988). These characteristics reflect the geologic history, the age of the dominant crust-forming event, and the age and characteristics of any superposed geologic events. In Arizona, where some of the world's great porphyry Cu deposits formed, distinct Paleoproterozoic basement terranes impart distinct Pb isotopic characteristics to the Mesozoic and Cenozoic igneous rocks intruded into the region and to associated hydrothermal systems (Bouse et al., 1999; Titley, 2001; Wooden et al., 1988). Their Pb isotopic characteristics reflect the igneous processes whereby magmas of low Pb concentration derived from the mantle assimilate crustal material as they rise into the shallow crust. Because the Paleoproterozoic crystalline crust and contemporaneous underlying mantle have isotopic compositions distinct from any much younger mantle-derived magma due to time-integrated growth of the three radiogenic daughter isotopes, assimilating only a small fraction of ancient crystalline crust can change the Pb isotopic composition of any magma and derived porphyry Cu hydrothermal system to values reflecting the values of the crustal column. The Paleoproterozoic lithospheric column underlying Arizona extends northeastward toward Bingham where the same high ^{207}Pb/^{206}Pb characteristics are recorded in the Pb isotopic compositions of hydrothermal fluids interpreted to reflect derivation from an enriched mantle source (Petke et al., 2010). The role of the crustal column in determining the Pb isotopic compositions of porphyry Cu deposits, particularly those of Phanerozoic age, cannot be overemphasized. The magma genesis process, combined with the isotopic composition of the rocks that the magma assimilates as it rises toward the surface, will ultimately dictate the overall Pb isotopic characteristics of that porphyry Cu system. As the hydrothermal fluid is derived from a well-mixed and homogeneous magma, the Pb isotopic composition of the high-temperature sulfide minerals is generally very uniform and reflects the averaging of all rocks encountered during magma genesis and during the formation of the porphyry deposit.

The relative contrast in Pb concentration and isotopic compositions between any magma or hydrothermal fluid and a rock that is assimilated or encountered during hydrothermal circulation provides an important constraint on the measured Pb isotopic composition of the rock or mineral. If there is little difference in their isotopic compositions, then there will be little change to the Pb isotopic composition during that interaction even if significant percentages of the rocks are assimilated or there is significant fluid–rock interaction. This isotopic compositional influence is clearly defined in the Andes where broad geographic and time-related changes in the Pb isotopic characteristic of magmas and hydrothermal systems emplaced from the Jurassic to the Pliocene are evident (Barreiro and Clark, 1984; Chiaradia and Fontbote, 2002; Kamenov et al., 2002; MacFarlane et al., 1990; Tosdal and Munizaga, 2003). Jurassic and early Cretaceous rocks emplaced close to the coast have Pb isotopic compositions that are crustal but reflect little interaction with ancient rocks, whereas rocks emplaced farther

east have noticeable input of older Pb isotopic compositions (Figure 4(a)). The Jurassic and early Cretaceous rocks were emplaced into a crustal column characterized by young mafic material with lower $^{207}Pb/^{204}Pb$ added during early continental margin extension, whereas the crust to the east consists of significant amounts of Paleozoic and older rocks with elevated $^{207}Pb/^{204}Pb$ that reflects time-integrated growth of a high U/Pb terrane (Coira et al., 1982; Jones, 1981; Tosdal and Munizaga, 2003).

Within the porphyry hydrothermal systems, the same two influences on the Pb isotopic compositions are evident. Many of the Peruvian and Chilean porphyry Cu deposits lying along and west of the eastern edge of the Mesozoic interarc rift system, known as the Domeyko fault system in Chile and the Incapucio fault system in southern Peru, are characterized by homogeneous Pb isotopic compositions regardless of paragenetic stage. The mafic rock-dominated crustal column is relatively young and has little Pb isotopic heterogeneity (Tosdal et al., 1999). To the east, Pb isotopic compositions of sulfides from various paragenetic stages show a considerable range and shift to much more variable compositions dominated by high $^{207}Pb/^{204}Pb$. A good example is shown by the Eocene El Salvador and Potrerillos porphyry Cu–Mo deposits and the Miocene porphyry Cu–Au and related quartz–alunite epithermal systems of the Maricunga belt in northern Chile. The high-temperature Cu–Fe sulfide minerals at El Salvador and

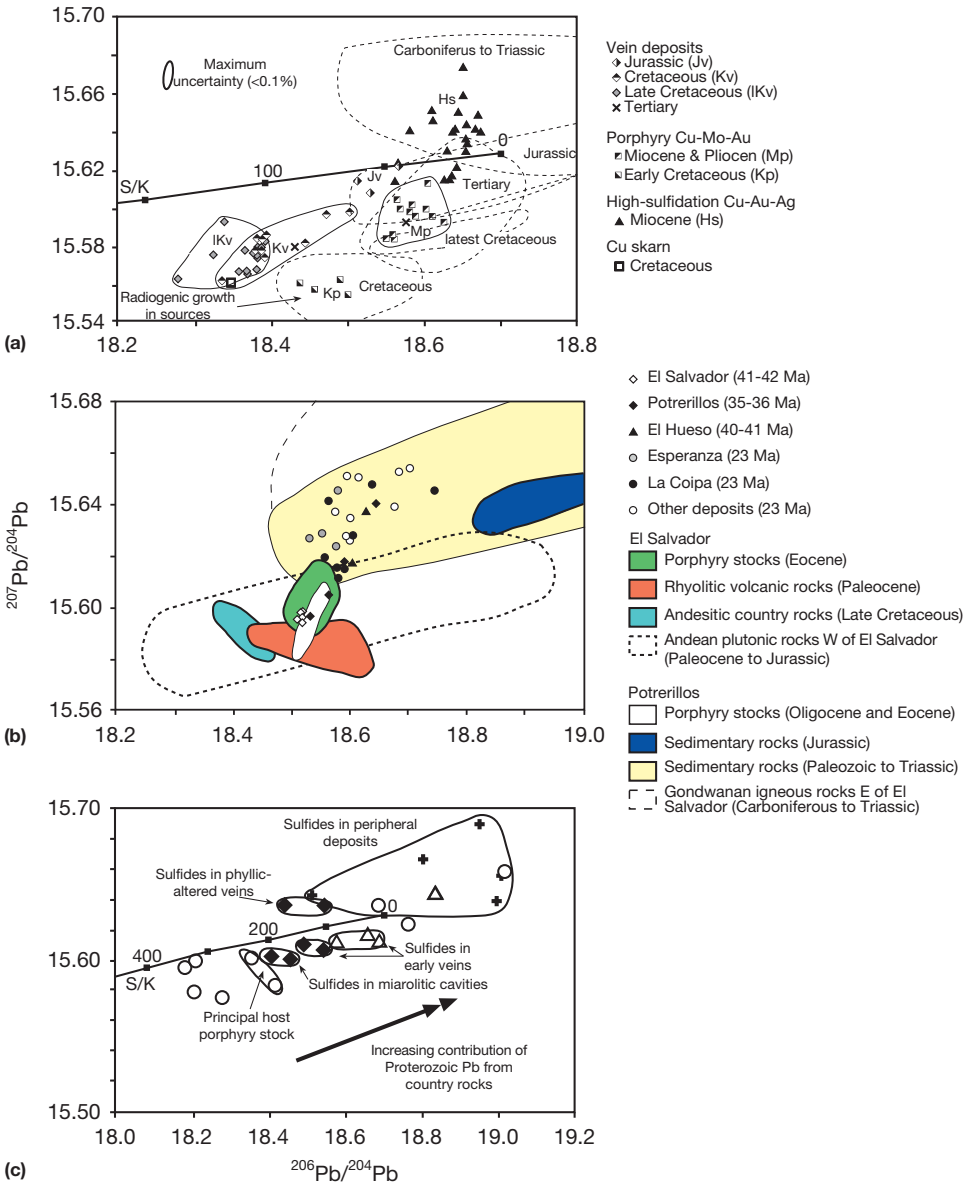

Figure 4 Variation in Pb isotopic compositions. (a) In central Chile, Pb isotopic compositions of igneous rocks and sulfide mineral vary systematically with age and geologic terrane (Tosdal and Munizaga, 2003). (b) In northern Chile, the Pb isotopic compositions of porphyry Cu-related hydrothermal systems reflect the underlying crustal column (Tosdal et al., 1999). (c) At the Bagdad porphyry Cu–Mo deposit, the Pb isotopic composition of sulfide minerals changes with paragenetic stage and reflects the incorporation of wall-rock Pb released during hydrothermal alteration from the Proterozoic country rock into the porphyry Cu-related sulfide minerals (Bouse et al., 1999; Tosdal et al., 1999).

Potrerillos have a limited range of Pb isotopic compositions that plot below the average crustal growth curves; these rocks were emplaced in a relatively young crustal column (**Figure 4(b)**). In contrast, the Miocene deposits to the immediate east in the Maricunga belt are characterized by very similar $^{206}Pb/^{204}Pb$ values but by elevated $^{207}Pb/^{204}Pb$ plotting above the average crustal growth curve. All these latter deposits are associated with intermediate composition magmatic rocks emplaced into Paleozoic rocks that are characterized by elevated $^{207}Pb/^{204}Pb$ (Tosdal et al., 1999). Shafiei (2010) documented similar crustal influences on Pb isotopic compositions of igneous rocks and porphyry Cu-related sulfide minerals in the Eocene and Miocene of Iran.

The effect of wall-rock composition is evident in some porphyry Cu hydrothermal systems. At El Salvador, there is no isotopic change through the different paragenetic stages, whereas the late sulfide minerals in Potrerillos show a Pb isotopic trend diverging from the composition of the porphyry intrusions and high-temperature Cu–Fe sulfide minerals toward higher $^{207}Pb/^{204}Pb$ values that are characteristic of the surrounding Paleozoic Gondwana crystalline basement (Thompson et al., 2004; Tosdal et al., 1999; **Figure 4(b)**). Similar evolution toward host rock Pb isotopic compositions are evident in porphyry Cu–Mo deposits in Arizona (Bouse et al., 1999; **Figure 4(c)**). Alternatively, distinct excursions in isotopic composition are evident in different paragenetic stages within the Rio Blanco–Los Bronces porphyry Cu–Mo deposits (Frikken et al., 2005). Although such effects are only visible where host rocks have a Pb isotopic contrast to the porphyry magmas, it seems evident that wall-rock Pb, released by hydrothermal reactions, may become dominant in Cu–Fe sulfide minerals precipitated late in the life of a system. Wall-rock Pb clearly dominates veins that form peripheral to and late in the overall magmatic and hydrothermal evolution of some deposits (**Figure 4(c)**; Bouse et al., 1999). Where this type of temporal evolution is not evident, it probably reflects a lack of distinctly different isotopic reservoirs rather than the absence of this evolutionary pattern.

13.14.7 Fluid Inclusions

Chapter 13.5 provides a comprehensive review of fluid inclusion systematics in porphyry deposits, and so only a cursory review is provided here. Fluid inclusions are the key source of information on the physical and chemical properties of fluids involved in porphyry-related hydrothermal processes and are central to current models for porphyry ore genesis. Fortunately, fluid inclusions are abundant in many porphyry deposits, particularly in the central quartz vein stockwork. It can, however, be difficult to constrain the timing of fluid inclusion formation relative to vein growth. Episodic fluid migration through individual fracture arrays causes veins to reopen and seal, resulting in multiple episodes of mineral growth, dissolution, and microfracturing, ultimately producing a complex array of primary and secondary fluid inclusions within annealed quartz grains. However, recent technological advances have improved the capacity to constrain the timing of fluid inclusion formation. Starting with a well-established framework of vein crosscutting relationships, the application of traditional fluid inclusion petrography techniques (e.g., Beane, 1982; Cooke and Bloom, 1990; Eastoe, 1978; Nash, 1976; Reynolds and Beane, 1985; Roedder, 1971, 1984) can now be combined with analysis of cathodoluminescence images of quartz textures obtained by scanning electron microscopy. This combination of techniques allows for unambiguous recognition of fluid inclusion assemblages in quartz that are associated with discrete mineralizing events (e.g., Landtwing et al., 2010; Rusk et al., 2008; Seo et al., 2012; Vry et al., 2010).

In some porphyry deposits, the earliest and deepest-seated veins contain high-temperature (>500 °C) two-phase (liquid + vapor) vapor-rich fluid inclusions that have moderate salinities (5–15 wt% NaCl equivalent); these are inferred to be low- to intermediate-density primary magmatic–hydrothermal fluids that exsolved from the crystallizing intrusive complex (e.g., Landtwing et al., 2010; Redmond et al., 2004; Seo et al., 2012; see **Chapter 13.5**). More commonly, the earliest-formed fluid inclusion assemblage observed in the quartz vein stockwork consists of coexisting high-temperature, low-salinity (<10 wt% NaCl equivalent) vapor + liquid inclusions that homogenize to vapor and saline inclusions that contain liquid + vapor + salt crystals + other daughter minerals that homogenize to liquid and typically have salinities of 30–50 wt% NaCl equivalent. This fluid inclusion assemblage, where vapor-rich and brine inclusions coexist in growth zones or secondary trails, implies trapping on the two-phase curve (see **Chapter 13.5**; Bodnar et al., 1985) and may reflect either separation of vapor from a liquid-like supercritical fluid (boiling) or condensation of a liquid, often of high salinity, from a vapor-like supercritical fluid. Late-stage veins may contain fluid inclusion assemblages that consist of low-temperature two-phase (liquid + vapor) low-salinity fluid inclusions of intermediate to high density. These typically homogenize to liquid, but some vapor-rich inclusions may be present that homogenize to vapor. Such assemblages are indicative of boiling of low-salinity water.

Synthetic fluid inclusion studies have provided a basis for the interpretation of fluid inclusion assemblages in porphyry deposits. In their study of phase relationships in the H_2O–NaCl system to 1000 °C and 1500 bars, Bodnar et al. (1985) demonstrated that some porphyry copper systems formed under P–T conditions such that any aqueous phase released from a magma must have exsolved as coexisting high-density brine and low-density vapor. Porphyry intrusions emplaced at greater depths (i.e., higher pressures) will not be in the fluid immiscibility field for H_2O–NaCl, and so they will only exsolve a vapor-like supercritical fluid. In this case, the earliest vein stages would preserve moderate-salinity (≈5–15 wt%) vapor-rich high-temperature inclusions, because phase separation or condensation has not occurred.

During the past two decades, microanalysis of fluid inclusions using laser ablation ICPMS (e.g., Audétat et al., 1998, 2008; Heinrich et al., 1999; Landtwing et al., 2010; Seo et al., 2012; Ulrich et al., 1999; Wilkinson et al., 2008) and PIXE techniques (e.g., Harris et al., 2003; Heinrich et al., 1992; Wolfe and Cooke, 2011) has provided compositional data not previously available to researchers of porphyry deposits. These studies have identified extreme (wt%) base metal concentrations in some high-temperature brines, vapors, and intermediate-density

supercritical fluids (see Chapter 13.5) and have stimulated debates regarding the main transporting agent for metals in porphyry vein stockworks (brine or vapor; e.g., Heinrich et al., 1999, 2004; Klemm et al., 2007; Landtwing et al., 2010; Pudack et al., 2009; Seo et al., 2012; Wilkinson et al., 2008; William-Jones and Heinrich, 2005; Wolfe and Cooke, 2011).

13.14.8 Conventional Stable Isotopes

Oxygen–deuterium and sulfur isotopic studies have provided important insights into the sources of mineralizing fluids and ore-forming processes in porphyry deposits. These studies have been facilitated by the widespread spatial distribution of sulfides, sulfates, and hydrous alteration minerals that occur in and around the central mineralized intrusive complex. In contrast, carbon–oxygen isotopic studies of carbonate minerals have been more limited in scope, due to the restriction of carbonate veins and alteration minerals to the propylitic halos of most porphyry deposits. The fundamentals of stable isotope geochemistry are presented in Chapter 6.3.

13.14.8.1 Oxygen–Deuterium

Taylor (1997), Vikre (2010), and Chapter 6.3 have reviewed the oxygen–deuterium isotopic systematics of porphyry deposits. Minerals precipitated early in the life cycle of a porphyry deposit (e.g., biotite) typically preserve magmatic O–D isotopic compositions (e.g., Harris et al., 2005; Hedenquist et al., 1998; Figure 5(a) and 5(b)). In contrast, depending on the paleolatitude, late-stage micas and clays can record some evidence for ingress of external fluids into the magmatic–hydrothermal domain (Sheets et al., 1996; Taylor, 1997; Figure 5(c)). This oxygen and deuterium isotopic evidence led to the model of H-ion metasomatism (e.g., phyllic alteration and related D-veins) being related to late-stage ingress of meteoric groundwater after the collapse of the magmatic–hydrothermal system (e.g., Gustafson and Hunt, 1975; Sheppard et al., 1969, 1971; Taylor, 1974). However, other workers have demonstrated a magmatic origin for late-stage muscovite and illite alteration in porphyry deposits (e.g., Harris and Golding, 2002; Hedenquist et al., 1998; Kusakabe et al., 1984, 1990; Watanabe and Hedenquist, 2001; Figure 5(c)).

Some debate has focused on whether the original (*c.*1970s) isotopic studies overemphasized the importance of meteoric water, possibly due to sampling problems (e.g., isotopic exchange during supergene processes). At the El Salvador Cu–Mo porphyry deposit, Chile, hydrothermal activity produced early potassic, then intermediate argillic and phyllic assemblages, and finally late-stage advanced argillic alteration assemblages (Gustafson and Hunt, 1975). Based on O–D stable isotopic analyses, Watanabe and Hedenquist (2001) reported a significant component of magmatic water (>90%) and only a minor meteoric component (<10%) in the waters that precipitated late-stage muscovite (Figure 5(c)). They interpreted the O–D isotopic compositions of alunite and pyrophyllite to indicate formation by condensation of magmatic vapors into groundwater.

In contrast to the results of Watanabe and Hedenquist (2001), there is D-isotope evidence for a meteoric component in both the early magmatic–hydrothermal fluids and late-stage waters in the Eocene porphyries of the Babine Lake area of British Columbia (Sheets et al., 1996). The meteoric component is envisaged to have been derived by (1) influx of evolved meteoric fluids into the melt at some depth below the site of ore formation or (2) by crustal assimilation of D-depleted country rock. Similar, D-depleted hypersaline fluids have been reported from the Copper Canyon porphyry system, Battle Mountain, Nevada (Batchelder, 1977). However, Taylor (1997) attributes these low δD values from biotite to overprinting by late-stage fluids. Bowman et al. (1987) provided stable isotopic evidence for mixing of magmatic waters with connate brines on the margins of the Bingham Canyon porphyry Cu–Au–Mo deposit. Cooke et al. (2011) demonstrated a progressive decrease in $^{18}O_{H_2O}$ values with time for quartz and carbonate gangue, providing evidence for an evolution from predominantly magmatic to meteoric waters in the Ampucao porphyry Cu–Au and Acupan epithermal Au–Ag veins, Philippines (Figure 5(d)–5(h)). These studies provide evidence for fluid mixing peripheral to porphyry mineralizing centers.

The O–D systematics of porphyry deposits are easily perturbed by late-stage hydrothermal activity and/or weathering and, therefore, need to be evaluated on a case-by-case basis, with analyses undertaken within a framework of detailed paragenetic sampling. A magmatic–hydrothermal origin for late-stage phyllic alteration helps to explain significant Cu endowment in veins related to this alteration stage (e.g., El Teniente; Cannell et al., 2005; Vry et al., 2010). A meteoric origin may be valid in other deposits, where phyllic-stage veins are barren.

13.14.8.2 Sulfur

Field et al. (2005), Rye (2005), Vikre (2010), and Chapter 6.3 have reviewed the sulfur isotopic characteristics of sulfides and sulfates from porphyry deposits. Sulfide and sulfate minerals coexist in parts of many porphyry deposits, particularly in the potassic and advanced argillic alteration zones, providing opportunities to investigate sulfate–sulfide fractionation phenomena (e.g., Rye, 1993; Rye et al., 1992). $\delta^{34}S_{sulfide}$ values from porphyry deposits are typically near 0‰ (Figure 6), with lower (negative) $\delta^{34}S_{sulfide}$ values typically related to deposition of sulfides from a sulfate-dominant (oxidized) fluid (Rye, 1993; Wilson et al., 2007a). Excursions to higher (positive) $\delta^{34}S_{sulfide}$ values can be attributed to variations in the bulk sulfur isotopic composition of the magma, either due to varied contributions to the overall magmatic sulfur budget of sulfur derived from the mantle, subduction zone fluids, seawater, or wall-rock assimilation (e.g., Sasaki et al., 1984; Vikre, 2010; see Chapter 6.3).

Sulfur isotopic compositions from selected porphyry deposits and districts are summarized in Figure 6. Although magmatically derived sulfides should have isotopic compositions around 0‰, several deposits have sulfides with distinctly negative $\delta^{34}S_{sulfide}$ values (as do high-sulfidation epithermal Au deposits). This group of deposits includes the Dinkidi alkalic porphyry Cu–Au deposit, Philippines (Wolfe and Cooke, 2011), the alkalic porphyry Cu–Au deposits of NSW (Heithersay and Walshe, 1995; Wilson et al., 2007a) and of British Columbia (Deyell and Tosdal, 2005), and also several calc-alkaline porphyry deposits from Chile and the southwestern United States (e.g., Ohmoto and Rye, 1979; Taylor, 1987;

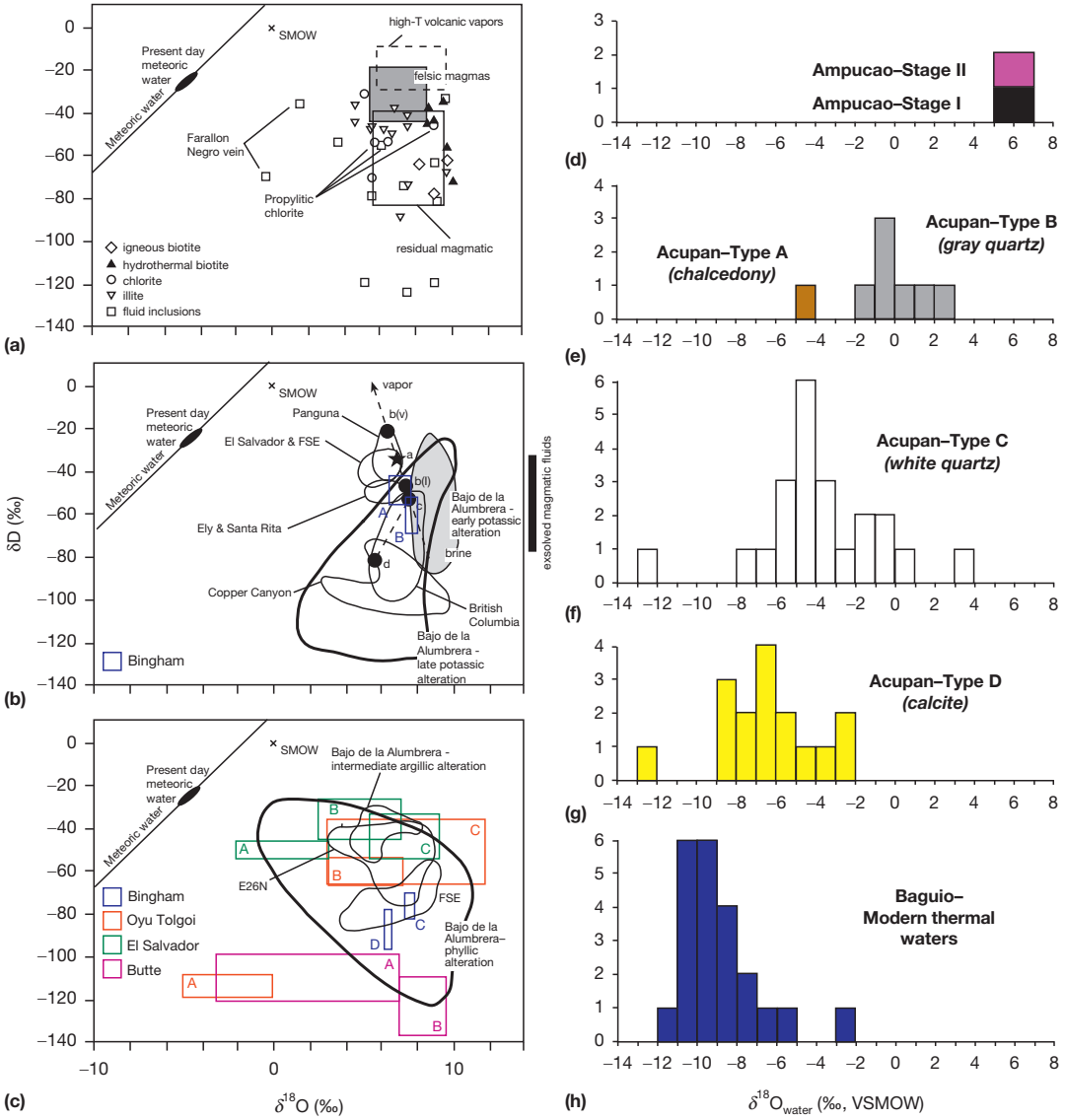

Figure 5 Oxygen–deuterium isotopes. (a) Calculated $\delta^{18}O$ and δD values of fluids responsible for different alteration assemblages at the Bajo de la Alumbrera porphyry copper–gold deposit (Harris et al., 2005). Compositions are based on temperatures determined from fluid inclusion data. Ranges of residual magmatic water (i.e., that remaining in an intrusion after degassing and crystallization: Taylor, 1974), compositions of water initially dissolved in felsic melts (Taylor, 1992), and low-salinity vapor discharges from high-temperature volcanic fumaroles (Giggenbach, 1992) are also shown. (b) Isotopic compositions of fluids associated with potassic alteration (modified after Harris et al., 2005; Hedenquist et al., 1998; Vikre, 2010). Isotopic evolution associated with early (stage 1) and late (stage 2) potassic alteration at Bajo de la Alumbrera has been modeled numerically after Shmulovich et al. (1999). From a primitive starting composition (point a), a magmatic fluid evolves during phase separation or boiling to distinctly different isotopic compositions. Points b(v) and b(l) mark the resultant vapor and liquid compositions, respectively. Cooling of the brine liquid causes further modification of the primitive magmatic signature resulting in depleted hydrogen and oxygen isotope compositions (point c). If a new pulse of unevolved magmatic fluid is introduced into the system, the hotter magmatic fluid will flash and drive fractionation to a maximum (point d). Note the overlap of the isotopic compositions of fluid responsible for the stage 2 potassic alteration with those determined from other porphyry ore deposits. For the Bingham data, A = propylitic alteration and B = potassic alteration. Fields modified after Ohmoto (1986), Bowman et al. (1987), Hedenquist and Richards (1998), and Vikre (2010). (c) Isotopic compositions of fluids associated with intermediate argillic (stage 3) and phyllic (stage 4) alteration at Bajo de la Alumbrera, modified after Harris et al. (2005) and Vikre (2010). Compositional ranges for fluids associated with phyllic alteration are based on model fluid temperatures determined from inclusion data (i.e., between 200 and 400 °C) and overlap with isotopic fluid compositions determined from other porphyry ore deposits. Bingham: C = sericitic alteration, D = argillic alteration. Oyu Tolgoi: A = dickite alteration, B = muscovite alteration, C = alunite and pyrophyllite alteration. El Salvador: A = kaolinite and dickite alteration, B = alunite and pyrophyllite alteration, C = muscovite alteration. Butte: A = 'sericite,' B = biotite (early dark micaceous alteration). Fields from Bowman et al. (1987), Taylor (1997), Hedenquist et al. (1998), Watanabe and Hedenquist (2001), Harris and Golding (2002), Khashgerel et al. (2006), and Vikre (2010). (d–h) Histograms showing calculated $\delta^{18}O_{water}$ values (‰, VSMOW) for veins from the Ampucao porphyry Cu–Au deposit and the Acupan intermediate-sulfidation epithermal Au–Ag veins that overprint it (Cooke et al., 2011). (d) Ampucao porphyry-style quartz veins: potassic stage I (black bar), intermediate argillic stage IIa (pink bar). (e) Acupan epithermal veins: early-stage type A chalcedony (brown bars) and type B gray quartz (gray bars). (f) Acupan epithermal veins: main-stage type C white quartz. (g) Acupan epithermal veins: late-stage type D calcite; VSMOW, Vienna Standard Mean Ocean Water. (h) Compositions of modern geothermal waters from the Baguio district (note that Ampucao quartz has values consistent with magmatic water compositions). At Acupan, calculated $\delta^{18}O_{water}$ values are highest for the gold-rich type B gray quartz bands that occur on the vein margins, and calculated $\delta^{18}O_{water}$ values decrease to near-meteoric values in the central type D calcite bands, indicating an increase in the proportion of meteoric to magmatic water with time and/or decreasing amounts of isotopic exchange between meteoric waters and igneous wall rocks.

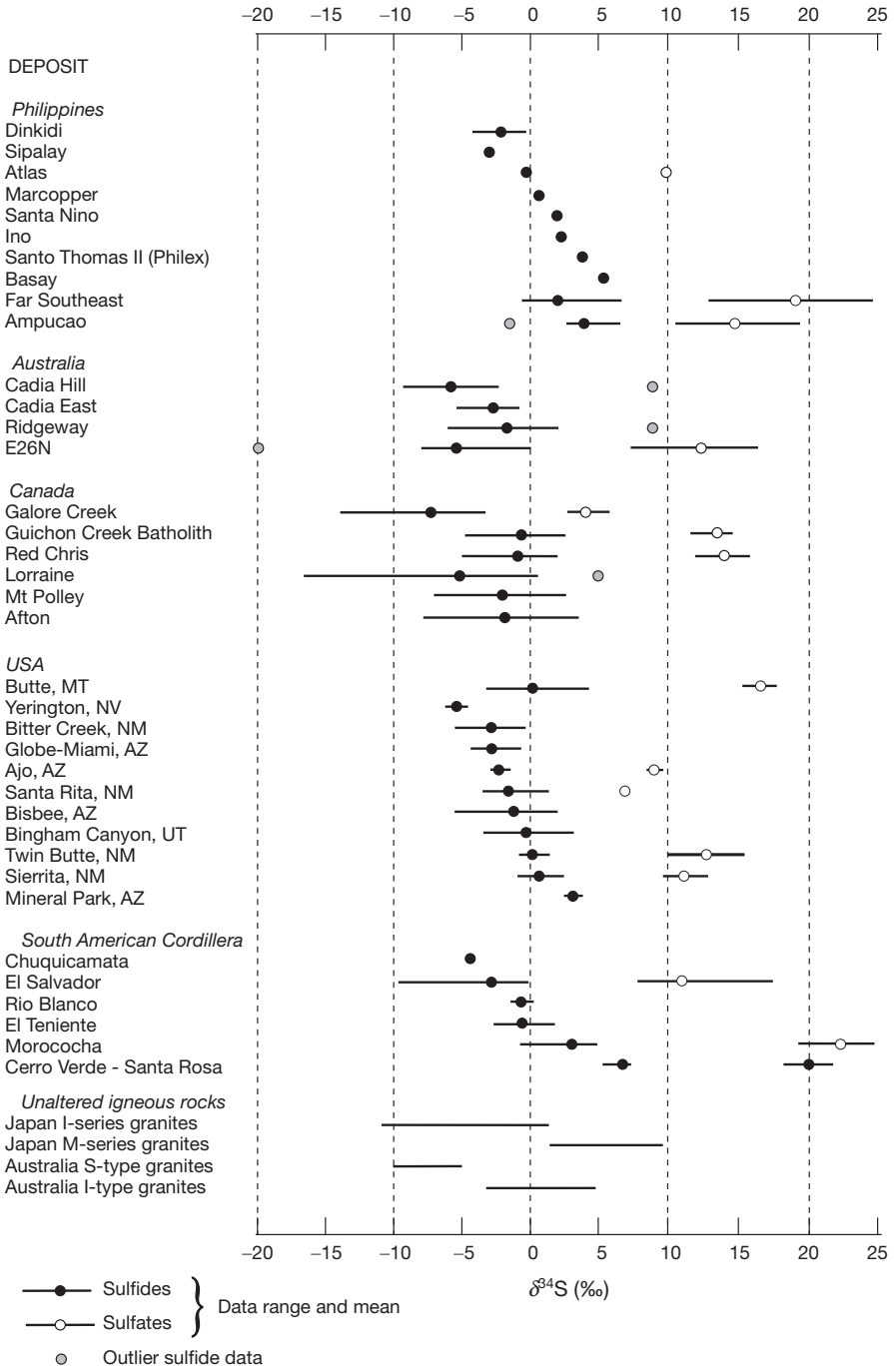

Figure 6 Ranges of $\delta^{34}S_{sulfide}$ values (per mil) determined for sulfide minerals from selected porphyry deposits and with granitic rocks (modified from Taylor, 1987; Wilson et al., 2007a; Wolfe and Cooke, 2011). Gray circles indicate outlier sulfide data. Data sources: Ohmoto and Rye (1979), Taylor (1987), Heithersay and Walshe (1995), Baker and Thompson (1998), Akira (2000), Lickfold (2002), Deyell and Tosdal (2005), Wilson et al. (2007a), Wolfe and Cooke (2011), and Cooke et al. (2011).

Figure 6). Sulfides at Dinkidi have lower $\delta^{34}S_{sulfide}$ values than other Philippine porphyry Cu–Au deposits (**Figure 6**; Cooke et al., 2011; Imai, 2001; Sasaki et al., 1984). The elevated $\delta^{34}S_{sulfide}$ values in most of the Philippine deposits have been interpreted to represent a seawater sulfur contribution to the hydrothermal fluids (Sasaki et al., 1984). The negative $\delta^{34}S_{sulfide}$ values at Dinkidi preclude seawater involvement; instead, the range of data is more consistent with an oxidized magmatic source of sulfur (e.g., Rye, 1993; Wilson et al., 2007a).

Sulfur isotopic studies provide useful insights into the sulfur budget of, and sulfur speciation within, porphyry deposits. Highly oxidized degassing magmas release $SO_{2(g)}$.

Sulfur dioxide can disproportionate at temperatures around 450–350 °C, producing approximately 3 moles of SO_4^{2-} for every mole of H_2S (e.g., Rye, 1993; Rye et al., 1992). If this process is the primary source of $H_2S_{(aq)}$ in porphyry deposits, then sulfate should be the dominant form of aqueous sulfur in the mineralizing fluids. However, numerous paragenetic studies have demonstrated that sulfides predominate over sulfates in the ores and altered rocks (e.g., Cannell et al., 2005; Seedorff et al., 2005; Vry et al., 2010; Wilson et al., 2003). The excess SO_4^{2-} produced by $SO_{2(g)}$ disproportionation may flux to the near-surface environment. Alternatively, inorganic sulfate reduction may occur in the porphyry environment, helping to generate the additional H_2S needed to precipitate the significant volumes of bornite, chalcopyrite, and pyrite that characterize porphyry deposits (e.g., Wilson et al., 2007a).

13.14.8.3 Carbon–Oxygen

Apart from the propylitic alteration zone, carbonate-bearing veins are a minor, late-stage component of most porphyry deposits due to the prevailing acidic conditions. Consequently, there are only limited C–O isotopic data. Sheppard et al. (1971) found that vein carbonates at Santa Rita, New Mexico, have $\delta^{13}C$ values of −2.5‰ to −5.9‰, slightly higher than igneous carbonates (−5‰ to −8‰). Sheets et al. (1996) identified a correlation between $\delta^{13}C$ values of carbonate vein minerals and δD values of inclusion fluids in the Babine Lake porphyry deposits. This correlation was used to confirm an early, CO_2-bearing meteoric component in the mineralizing fluids.

In contrast to calc-alkaline porphyry systems, alkaline porphyry deposits (e.g., NSW and British Columbia) can have a significant component of carbonate in the early copper-mineralized veins (e.g., quartz–bornite–carbonate veins at Northparkes and Cadia; Lickfold et al., 2003; Wilson et al., 2003). Pass et al. (in press) provide the first detailed analysis of C–O systematics of carbonate veins and breccia cement in a silica-undersaturated alkalic porphyry Cu–Au deposit. Their study of the Mt Polley porphyry Cu–Au deposit, British Columbia, has identified enriched C–O isotopic values that are not consistent with simple precipitation of carbonate veins and breccia cement from an entirely magmatic source of hydrothermal fluid. Pass et al. (in press) argue for a model of wall-rock carbonate assimilation by the mineralizing intrusions in order to explain both the C–O systematics of the hydrothermal assemblages and the silica-undersaturated nature of the monzonite complex.

13.14.9 Nontraditional Stable Isotopes

Over the past decade, new insights into the mobilization, transport, and deposition of metals in ore deposits have been made possible by the development and application of nontraditional stable isotope systems (Johnson et al., 2004; see **Chapter 6.3**). This rapidly evolving field has involved the study of the isotopic variability of many ore metals, including Cr, Fe, Cu, Zn, Mo, Sn, and Hg. In porphyry systems, applications of nontraditional stable isotopes are limited. Most research has focused on the principal ore metal Cu, within both the hypogene and supergene domains. In addition, studies have attempted to identify zoning patterns that might reflect temperature, redox, or other controls that could be of use in mineral exploration. Limited data are available for Fe and Mo in porphyry deposits, and there are no studies to date of the isotopic composition of Zn or other accessory metals.

Limited isotopic variation might be anticipated in the hypogene porphyry environment because of the typically small equilibrium isotope fractionation at elevated temperatures and restricted variation in redox state for elements such as Cu and Fe. Nonetheless, the high precision of measurements (<0.1‰) has allowed small but systematic variations to be resolved. In contrast, greater variability is predicted at lower temperatures and where changes in the oxidation state of metals can induce large fractionations. Such conditions typify the supergene environment, and the greatest variability in the isotopic composition of Cu in any terrestrial environment has been recorded here.

13.14.9.1 Copper

Two stable isotopes of copper exist, ^{63}Cu and ^{65}Cu, with isotopic abundances of 69.174% and 30.826%, respectively (Shields et al., 1964). For this article, 693 measurements of the isotopic composition of Cu in hydrothermal systems are compiled, derived from native Cu, sulfides, and oxides, plus a few related analyses of trace Cu-bearing secondary minerals (e.g., goethite). These data include measurements on sulfides and oxides from active submarine hydrothermal deposits, volcanic-hosted massive sulfide deposits, skarn deposits, and other hydrothermal ore types. About half of the data (334) come from porphyry systems, mostly from four studies (Graham et al., 2004; Larson et al., 2003; Li et al., 2010; Mathur et al., 2005), divided mainly between Cu–Au (263) and Cu–Mo (67) subtypes. Of the Cu–Mo data, about half of the results are from supergene minerals (Mathur et al., 2009).

The isotopic composition of Cu in hypogene sulfides (mostly chalcopyrite; some bornite) from porphyry deposits shows little variation, with $\delta^{65}Cu$ values mostly between −0.1‰ and +0.5‰ relative to the NIST SRM976 Cu standard (**Figure 7**). The average value for hypogene sulfides from the Cu–Au systems is slightly higher ($\delta^{65}Cu = 0.30‰$) than from the Cu–Mo systems (0.16‰, omitting two outliers). If one ignores the possibility of analytical artifacts derived from the laser ablation method used in one study (Graham et al., 2004), hypogene compositions appear to be more variable in the Cu–Au systems (−1.67‰ to +1.64‰) than in the Cu–Mo deposits (−1.16‰ to +0.95‰).

The homogeneity of hypogene Cu isotope compositions in porphyry systems may limit the use of this isotopic system for identifying different sources of Cu (e.g., Hoefs, 2009) and tracing depositional processes. Despite this, some zoning patterns have been observed and interpreted in terms of a range of fractionation and mixing processes during mineralization. In a study of the Grasberg Cu–Au system, Graham et al. (2004) found evidence for a progressive enrichment in ^{65}Cu through three major phases of igneous intrusion. They speculated that this was due to 'distillation' from the same deeper source, inferring Cu transport in a vapor phase enriched in ^{63}Cu and consequent evolution of the deeper (presumed closed) system

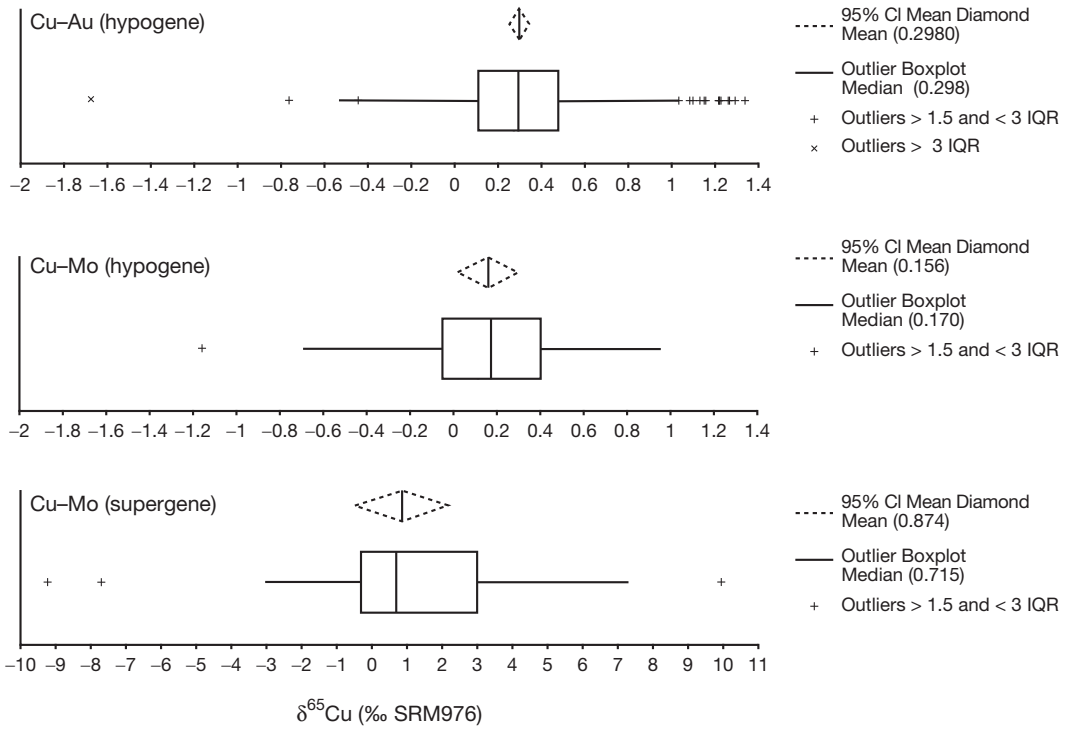

Figure 7 Copper isotope data from porphyry systems.

to higher δ^{65}Cu with time. The preferential fractionation of light copper isotopes into the vapor is supported by experimental data (Maher et al., 2011) but contradicted by quantum chemical calculations of equilibrium fractionation assuming vapor phase Cu_3Cl_3 or $CuCl(H_2O)$ (Seo et al., 2007). However, copper sulfide species such as $Cu(HS)_2^-$ have been proposed as the most likely agents for vapor transport in natural systems (e.g., Pokrovski et al., 2008), and the quantum calculations do not take into account possible kinetic enrichment of light isotopes in the vapor, so vapor enrichment in ^{63}Cu is more likely.

In a study of the Northparkes alkalic porphyry Cu–Au system in the Cadia district of New South Wales, Australia, Li et al. (2010) found small but systematic Cu isotope variations in four drill cores that extended from the inner ore zones (K-feldspar, K-feldspar–biotite, and biotite–magnetite alteration) outward into the peripheral zones (hematite–sericite–carbonate or phyllic/propylitic alteration) of two separate mineralized centers. In general, δ^{65}Cu values in the high-grade cores cluster close to 0.2‰, but although a lot of the data overlap within error, there appeared to be a consistent shift to a minimum of −0.4‰ to −0.8‰ on the margin of the potassic zone and then a general increase upward/outward to +0.2‰ to +0.8‰. A similar decrease in δ^{65}Cu (from ~0.6‰ to ~0.0‰) was also described with increasing distance (to about 400 m) from the Grasberg intrusive complex (Graham et al., 2004). The variations at Northparkes are not coupled to δ^{34}S values indicating that Cu isotopes are not fractionated by the fluid temperature and redox gradients that control the δ^{34}S zoning observed in these systems (Wilson et al., 2007a). The pattern was modeled in terms of equilibrium Rayleigh fractionation during cooling-driven precipitation that produced a negative shift in $\delta^{65}Cu_{sulfide}$ (negative $\Delta^{65}Cu_{fluid-sulfide}$) outward through the ore zone, combined with an increasing contribution of relatively ^{65}Cu-enriched country rock-derived Cu on the fringe of the deposit (Figure 8). Although viable, the model is one of a number of possible alternatives that also include fractionation and dispersion of Cu by ^{65}Cu-enriched vapor (producing the upper, high-$\delta^{65}Cu_{sulfide}$ halo) and ^{65}Cu-depleted brine (producing the inner, high-grade, low-$\delta^{65}Cu_{sulfide}$ core).

In the supergene weathered parts of Cu–Mo systems, δ^{65}Cu in native copper, secondary sulfides, oxides, carbonates, silicates, and leached cap material vary from −9.25‰ to 9.98‰ (omitting one outlier; Figure 7) with an average of 0.94‰ ($n = 28$). This wide range points toward the importance of redox cycling of copper as a major fractionation mechanism, and this control has been confirmed by experiments. Given the importance of oxidation and re-reduction of copper in the supergene enrichment process, the measurement of copper isotope compositions is likely to provide valuable new insights into these processes.

Most supergene sulfides are enriched in ^{65}Cu relative to the average hypogene value of 0.16‰ indicating fractionation during partial leaching. The more extreme negative values are derived from hematite (−goethite) boxwork samples (Mathur et al., 2009), consistent with more extensive leaching and fractionation in these rocks. Single analyses of atacamite and cuprite have negative values; native Cu and chrysocolla may have negative or slightly positive δ^{65}Cu (−3.03‰ to 1.26‰), and copper oxides, azurite, turquoise, malachite, and the principal secondary sulfide chalcocite are invariably isotopically heavy (>2.02‰, excluding one low chalcocite value). This pattern broadly corresponds to the oxidation state of copper in these minerals, with those containing Cu^{2+} tending to be enriched in ^{65}Cu.

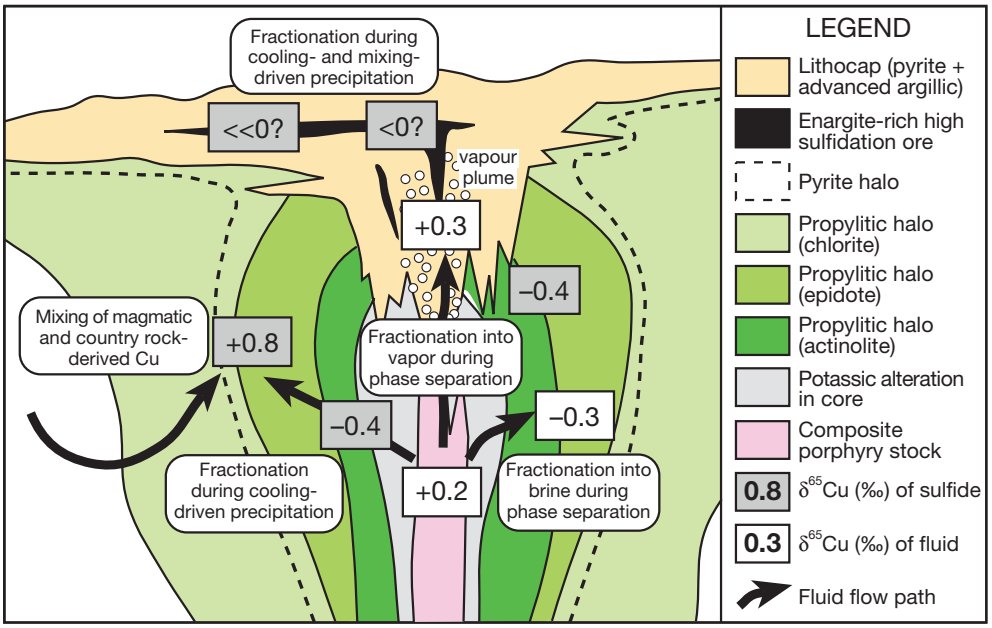

Figure 8 Cartoon illustrating possible mechanisms and extent of isotopic fraction of copper in porphyry systems. Based on the vapor fractionation model of Seo et al. (2007) and isotopic variations as discussed by Li et al. (2010).

Experimental studies (Ehrlich et al., 2004) have shown a significant fractionation of ~3‰ between aqueous Cu^{2+} and covellite, suggesting that partial oxidative leaching of sulfides could produce solutions with $\delta^{65}Cu$ several per mil higher than the hypogene minerals. Complete or near-complete reduction/precipitation of this copper as secondary oxides or sulfides in the enrichment blanket of porphyry copper deposits would result in this isotopically heavy signature being preserved. This mechanism was invoked by Braxton and Mathur (2011) to account for elevated $\delta^{65}Cu$ values in secondary chalcocite and djurleite at Bayugo, Philippines. Extreme enrichments (>6‰) in this environment (exotic zone) were explained by repeated cycles of oxidative dissolution and reprecipitation during maturation of the enrichment profile in parallel with a descending water table. Significantly, Braxton and Mathur (2011) also documented a lateral decrease in $\delta^{65}Cu$ from >+3‰ in the proximal exotic zone to <+1‰ in the distal exotic zone, explained in terms of extraction of Cu from a leached cap progressively depleted in ^{65}Cu by the aforementioned mechanism. Such zoning patterns in exotic secondary sulfides could provide indications of proximity and direction to the source area in porphyry systems.

13.14.9.2 Molybdenum

Molybdenum has seven stable isotopes with atomic masses (abundances) of 92 (15.86%), 94 (9.12%), 95 (15.70%), 96 (16.50%), 97 (9.45%), 98 (23.75%), and 100 (9.62%; Hoefs, 2009). Both $\delta^{97}Mo$ and $\delta^{98}Mo$ values (ratios relative to ^{95}Mo) have been reported in the literature. Limited work has been done on molybdenum isotope systematics in porphyry environments, but the insights this technique may provide on transport and precipitation mechanisms will mean that this will no doubt increase in future.

Few data exist on the molybdenum isotope composition of igneous rocks, but several analyses of basalts and granites display a narrow range of $\delta^{97}Mo$ close to 0 (relative to the Rochester JMC Mo standard), suggesting that igneous fractionation is limited (Anbar, 2004). Low-temperature fluids from mid-ocean ridge flanks have $\delta^{97}Mo$ ~0.5‰ (McManus et al., 2002), which is higher than igneous rocks but lower than seawater pointing to the operation of fractionation processes during lower temperature fluid–rock interaction and transport. This is supported by the ~1‰ variation observed in molybdenite samples from a variety of (undescribed) ore deposit types (Barling et al., 2001; Wieser and de Laeter, 2003).

At the time of writing, only 19 samples of molybdenite from porphyry ore deposits have been analyzed (Highland Valley, Canada; Mount Tolman, United States; Los Pelambres, El Teniente, Andacollo, Inca de Oro, and Collahuasi, Chile; Grasberg, Irian Jaya; and Oyu Tolgoi, Mongolia). These have $\delta^{97}Mo$ values between −0.53‰ and +0.53‰ (Hannah et al., 2007; Mathur et al., 2010; Pietruszka et al., 2006), both higher and lower than likely igneous sources. Significant variation was observed within single deposits (e.g., 0.5‰ at El Teniente; Mathur et al., 2010), implying that local igneous and/or hydrothermal processes are likely to be the key controls of isotopic variations.

Hannah et al. (2007) speculated that the variation observed in high-temperature hydrothermal deposits could be related to Rayleigh distillation during molybdenite precipitation from the vapor phase. This mechanism is supported by experimental studies, which showed that fractionation between MoO_4^{-2} and $MoO_3 \cdot nH_2O$ can occur in high-temperature aqueous systems (Tossell, 2005). If correct, zoning in the isotopic composition of molybdenite might be expected in porphyry environments, providing a potential tool for tracing flow pathways. However, fluid inclusion data show that the highest

molybdenum concentrations are found in the brine phase (e.g., Wilkinson et al., 2008) raising doubts about the importance of vapor transport and related fractionation processes. Clearly, many more experimental and carefully constrained field studies are required before there is a clear picture of the likely extent and controls of molybdenum isotope fraction in porphyry systems.

13.14.9.3 Iron

Iron has four naturally occurring stable isotopes: ^{54}Fe (5.84%), ^{56}Fe (91.76%), ^{57}Fe (2.12%), and ^{58}Fe (0.28%). Both ^{56}Fe/^{54}Fe and ^{57}Fe/^{54}Fe ratios are reported in the literature as δ^{56}Fe and δ^{57}Fe, respectively, most commonly relative to the IRMM-014 standard but also in some cases to average igneous rock (Beard and Johnson, 2004). Terrestrial igneous rocks are remarkably homogeneous in their iron isotope composition, with a mean $\delta^{56}Fe_{IRMM\text{-}014}$ of 0.09 ± 0.05‰. However, it is worth noting that only 22 analyses of continental silicic rocks were available at the time of the compilation of Beard and Johnson (2004).

Iron isotope data exist only from two porphyry systems. In their study of Grasberg, Graham et al. (2004) reported a variation in $\delta^{56}Fe_{IRMM\text{-}014}$ of between −2.0‰ and 1.1‰ and a clear distinction between chalcopyrite (mostly −1.7‰ to −0.3‰) and pyrite (0.0–0.8‰) implicating mineralogical fractionation and/or precipitation at different temperatures or from different fluids. If liquid–vapor fractionation of Fe isotopes is an important process at Grasberg, it is possible that precipitation of the isotopically heavy pyrite occurred from an iron-enriched brine that was depleted in light isotopes. Alternatively, iron isotope compositions in the pyrite shell might reflect mixing between magmatic and country rock-derived iron (Graham et al., 2004).

In the Northparkes system, Li et al. (2010) reported iron isotope compositions from 13 chalcopyrite separates. Delta values, recalculated here to $\delta^{56}Fe_{IRMM\text{-}014}$, are in the range −0.27 to 0.51‰ with an average of 0.05‰. This was interpreted in terms of a single orthomagmatic source. Iron isotope systematics were decoupled from both copper and sulfur and showed no correlation with Cu grade or alteration assemblage. At present, it is not understood why there is a significant difference between the systems, and this is clearly an area that warrants further work.

13.14.9.4 Summary

The study of nontraditional stable isotopes in general and as applied to porphyry deposits in particular is at an early stage. It is apparent that wider variations in isotopic compositions are present in hydrothermal ore deposits than in any other terrestrial environments, which make them particularly interesting for further investigation. Several studies have inferred the probability of Rayleigh distillation processes in the systematic fraction of metals during precipitation of ore minerals. If this general process is confirmed, it will open up many possible applications, with the isotope systematics potentially tracking flow pathways through deposits and out into the outflow region, the domain of spent ore fluids.

At the present time, models to explain isotope fractionation patterns of ore metals in porphyry systems are underconstrained, particularly in the absence of experimental data on fluid–mineral fractionations and lack of knowledge on whether equilibrium or kinetic fractionations are likely to prevail. Consequently, current interpretations are somewhat speculative. Nonetheless, the data summarized here provide an indication of the types of new insights that studies of ore metal stable isotopes will provide. In time, these isotope systems are likely to provide powerful new tools for testing current models of metal transport and deposition in the porphyry environment. The operation of Rayleigh distillation processes may produce patterns that help unravel complex flow patterns. Mixing between magmatic and country rock-derived metals may be possible on the fringes of some systems if there is an isotopic contrast (such as for Cu in magmas intruding black shale). The probability of isotopic fraction of metals that can be transported in the vapor phase, such as Cu, Mo, As, Sb, and Li, may be key to an improved understanding of the evolution and distribution of liquid and vapor phases and their importance in metal transport and deposition. Vapor phase transport of copper into epithermal systems could induce an isotopic fingerprint that reflects the efficiency of the process and may distinguish epithermal mineralization that overlies fertile or barren porphyry deposits. The generation of isotopic zonation patterns by any of these processes could yield a useful tool for mineral exploration.

13.14.10 Ore-Forming Processes

Porphyry deposits begin with partial melting of the metasomatized mantle wedge, which generates hydrous oxidized magmas that can potentially transport metals and sulfur together to an upper-crustal magma chamber (e.g., Richards, 2003; **Figure 9(a)**). During magma ascent, if the melt becomes saturated with H_2S, chalcophile elements such as copper and gold will be sequestered by early-crystallizing sulfides or by an immiscible sulfide liquid. These will most likely be retained at the base of the crust and will not become involved in upper-crustal magmatic–hydrothermal processes. A high oxidation state of the magma is advantageous for chalcophile metal transport as this increases sulfur solubility as SO_2, thereby limiting sulfide crystallization prior to arrival at the trap site. Consequently, porphyry copper, gold, and molybdenum deposits tend to be associated with the most highly oxidized, magnetite series granitoids. The abundance of anhydrite in some porphyry systems (e.g., El Teniente, Chile; Cannell et al., 2005; Vry et al., 2010) reflects abundant SO_2 in the magmatic fluids, based on the sulfur isotopic compositions of the sulfate and coexisting sulfide minerals (**Figure 6**).

Once a shallow-crustal magma chamber is established (**Figure 9(b)**), porphyry ore genesis requires the release of large volumes of magmatic volatiles and metals from crystallizing porphyritic intrusions (the 'magmatic–hydrothermal transition'). Candela (1991) speculated that when magmas exsolve an aqueous phase, a 'foam' or 'froth' will accumulate between the solidified carapace and the central crystal mush. Volatiles are concentrated in this zone as bubbles, and if bubble density is high enough to provide connectivity, then they ascend buoyantly up the walls of the solidifying stock, accumulating in the apex of the intrusion, and potentially resulting in the growth of unidirectional solidification textures

(e.g., Lickfold et al., 2003; Wilson et al., 2003). Accumulation of fluids beneath the carapace of the inwardly crystallizing stock eventually leads to carapace failure, second boiling, and mineralized stockwork formation when vapor pressures exceed lithostatic pressure and the tensile strength of the crystallized carapace (Burnham, 1979, 1985; Burnham and Ohmoto, 1980). The fracture event may initially lead to increased volatile exsolution from the melt; however, fractures will subsequently seal due to mineral deposition and/or lithostatic compression. Cycles of volatile accumulation and fluid release result in multiple fracture events, producing the classic vein crosscutting relationships observed in porphyry deposits.

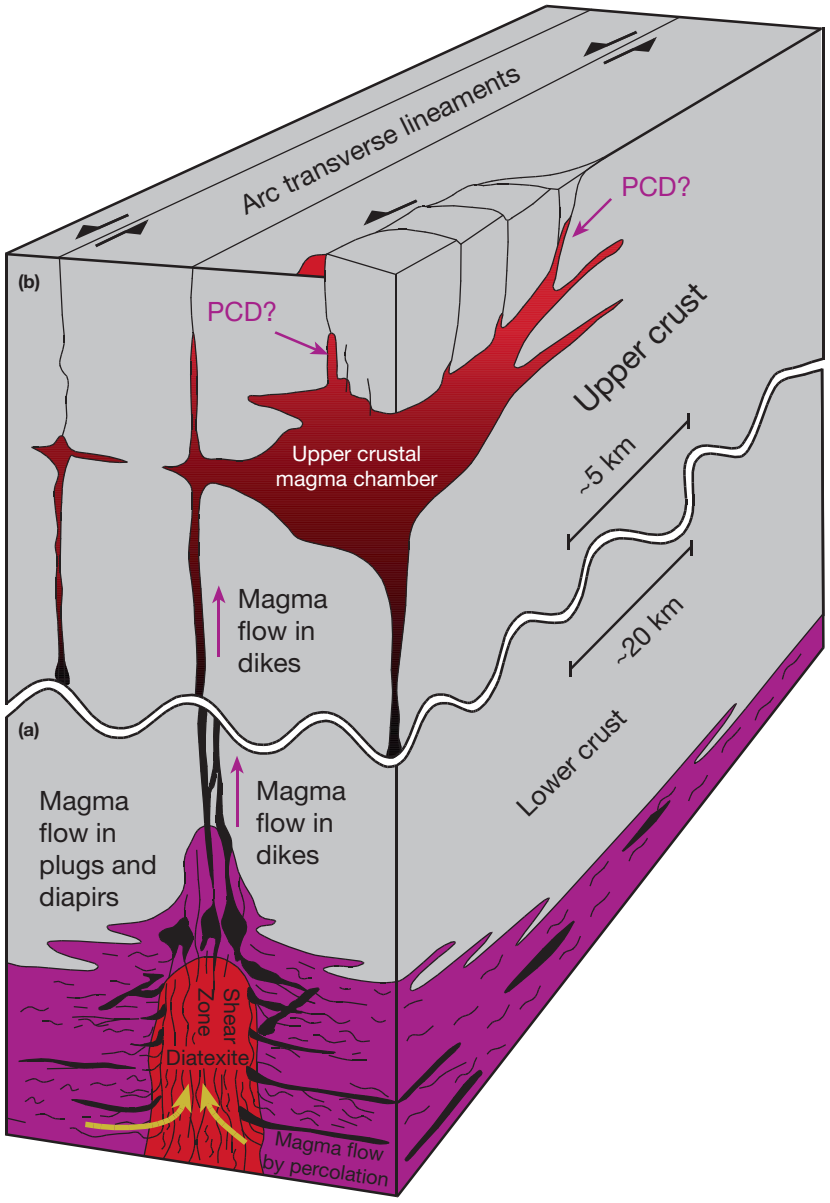

Figure 9 Schematic cross section of a translithospheric shear zone, modified from Richards (2003). (a) Migmatitic zone in the lower crust. The metatexite zones are where the region contains partial melt at volumes lower than the critical melt fraction, so that melts migrate by percolation to regions of lower pressure. Horizontal compression will cause the accumulation of melt in horizontal sills. Extensional shear bands can form due to localized shear strain, and melt will be drawn into these zones, rising as buoyant plugs or diapirs. These may coalesce into through-going dikes, providing a conduit for the transfer of melt from the base of the crust to the upper crust. (b) Magma migrates up dikes to its neutral buoyancy level. If the dikes connect to the surface, volcanism may occur (shown here as a red-colored dacite dome). Alternatively, magmas may accumulate within an upper-crustal magma chamber, particularly under a compressional tectonic regime, which suppresses volcanism and promotes uplift through basin inversion. Volatile exsolution during fractional crystallization can cause bubbles of volatiles to coalesce on the walls of the crystallizing magma chamber. Once connectivity is achieved, volatiles will migrant buoyantly to the apices of the magma chamber, where unidirectional solidification textures may form. Brittle failure will occur when vapor pressures exceed the combined effects of lithostatic load and the tensile strength of the surrounding rock mass, resulting in stockwork vein formation and ore deposition; PCD, porphyry copper deposit. *Note*: Richards' (2003) original model involves arc-parallel strike-slip faults, with magmatism localized within strike-slip pull-apart basins, in contrast to the inverted basin model and arc-transverse faults shown here.

The processes of ore deposition remain poorly understood in most porphyry deposits. It is remarkable that for such a well-studied class of hydrothermal ore deposit, such a fundamental question remains to be resolved adequately. Many workers propose models of ore formation based on fluid cooling (e.g., Klemm et al., 2007; Redmond et al., 2004; Rusk et al., 2008; Ulrich et al., 2002). While cooling is certainly capable of causing sulfide deposition, extreme temperature gradients are required for this process to generate ore grades. Such conditions are only achieved where fluids mix, most readily at the Earth's surface or with greater difficulty in the subsurface. Conductive cooling is slow, requires intimate fluid–rock contacts, and occurs slowly over large distances (Drummond and Ohmoto, 1985). None of these favor high-grade ore formation in fractured rock masses and are most likely to produce weak geochemical anomalies at best. For deposits where replacement-style sulfide mineralization predominates, water–rock interaction is implicitly involved as an ore-forming process. This is less important for most porphyry deposits, where the ores reside primarily in a fracture mesh. Other processes, such as depressurization, fluid mixing, boiling, and/or condensation, are required to promote high-grade ore formation in veins and hydrothermal breccias (see **Chapter 6.1**).

Porphyry deposits are huge accumulations of sulfur, with the central ore zone dominated by bornite and/or chalcopyrite ± gold, molybdenite, and in some cases chalcocite or enargite. The peripheral altered rocks can contain abundant pyrite, up to several volume percent of the rock mass (Lowell and Guilbert, 1970). Metal transport in the magma is favored by oxidizing conditions, with sulfur transported primarily as SO_2, to prevent formation of immiscible sulfide droplets and sequestration of copper–gold ores in the mantle. Ore formation therefore requires either (a) a sulfate reduction mechanism at the trap site (e.g., water–rock interaction), (b) a supply of external H_2S that mixes with the copper–gold-bearing fluids, or (c) a huge excess of sulfur flushing through the system, with much of the oxidized sulfur failing to precipitate at the trap site, and sulfides scavenging the smaller proportion of reduced aqueous sulfur produced by SO_2 disproportionation. Sulfur isotope studies typically indicate that the hydrothermal fluids forming porphyry deposits are oxidizing (SO_4^{2-}-predominant). Based on O–D isotopic evidence, option (b) seems unlikely in most cases, and so options (a) and (c) require more detailed investigation. Wilson et al. (2007a) provided evidence for sulfate reduction causing sulfide deposition coupled with hematite alteration in the Cadia porphyry Cu–Au deposits, providing support for option (a).

In contrast to ore formation, the processes of hydrothermal alteration are relatively well understood. Potassic and propylitic alteration assemblages form early, under lithostatic loads. The transition from potassic to propylitic alteration relates to increased water–rock interaction and wall-rock buffering out from the center of the hydrothermal system. O–D isotopic signatures from phyllic alteration assemblages confirm that both the early- and late-stage fluids are dominated by a magmatic component in many porphyry deposits (e.g., Harris and Golding, 2002; Kusakabe et al., 1984, 1990; Watanabe and Hedenquist, 2001; Wolfe et al., 1996). Transitions to late-stage acid alteration (phyllic and advanced argillic assemblages) therefore appear to correlate with a progression from lithostatic to hydrostatic load (e.g., Fournier, 1999), rather than to the late-stage ingress of meteoric water (e.g., Taylor, 1974). The same P–T change may cause metal deposition at depth, while at higher levels the resulting gas phase becomes more acidic and produces lower pH alteration.

It seems that the importance of late-stage waters varies from deposit to deposit (e.g., Bowman et al., 1987; Harris et al., 2005; Watanabe and Hedenquist, 2001). They disrupt alteration zonation patterns by creating domains of acid alteration (typically fault-controlled) that overprint earlier-formed potassic and propylitic assemblages (e.g., El Salvador, Chile, Gustafson and Hunt, 1975; Batu Hijau, Indonesia, Garwin, 2002). Another role may be to complicate the original ore shells by locally redistributing precious metals. Epithermal fluids typically have limited capacity for copper redistribution but potentially can dissolve significant amounts of gold and silver from porphyry Cu–Au deposits, because the solubility of precious metals as aqueous bisulfide complexes increases with decreasing temperature when aqueous H_2S contents remain high (Cooke and Simmons, 2000). Late-stage processes commence when the thermal anomaly around the crystallizing porphyritic stock collapses, allowing brittle failure of what were quasi-ductile rocks during the earliest alteration stage and the propagation of district-scale faults that may host epithermal mineralization. Such processes mark the end of porphyry ore formation and the beginning of peripheral ore deposit formation (e.g., epithermal and distal carbonate-hosted gold deposits).

13.14.11 Exploration Model

The overall characteristics of porphyry Cu deposits easily lend themselves to exploration. As they are largely the product of subduction of an oceanic plate beneath an overriding oceanic or continental plate or collisional orogens long after subduction of an oceanic plate has ceased, any exploration must focus on these geologic terranes. The magma is oxidized and hydrous and this will be reflected in the phenocryst mineralogy and in the igneous geochemistry. Porphyry intrusions directly associated with mineralization do not erupt (Cooke et al., 2007).

As there is a common theme of short- to long-lived magmatism (~1 to 10 My), evolving from early volcanism to main-stage plutonism as the magmatic arc wanes, porphyry Cu deposits generally form near the end of any magmatic episode and may form clusters of deposits, some of which are economic, whereas others are not. Significant examples include Oyu Tolgoi (Mongolia), Cadia (NSW), Atlas (Philippines), and Chuquicamata (Chile). There are many cases where two or more porphyry deposits are situated within 3 km of each other and may be derived from the same deep-seated magma chamber. The outer propylitic alteration halos of these groups of deposits generally overlap.

Fluid and magma escape from the upper-crustal chamber along a fracture and fault systems present in the roof rocks. Hydrothermal alteration associated with the magmatic–hydrothermal system imparts characteristic sulfide and silicate mineral assemblages that are generally distributed in predictable patterns (e.g., **Figure 1**). Accompanying these alteration assemblages are chemical changes in the rocks, which provide

important vectoring tools toward the mineralized core. However, the larger footprint, up to 10 km in horizontal dimension, to the porphyry Cu deposit is produced either by thermally driven circulation of external groundwaters (e.g., Bowman et al., 1987; Dilles et al., 2000) or by leakage of hydrothermal fluids from the roof of the much larger magma chamber that underlies the porphyry deposit and that ultimately sources most of the fluids and metals. Depending on temperatures, fluid, and wall-rock compositions, the peripheral waters can produce distinct changes in the rock mass, depending upon the depth within the porphyry Cu system. In volcanic wall rocks, minerals stable at higher temperatures characterize the inner propylitic assemblage (actinolite subzone; **Figure 1**), becoming more abundant as the porphyry deposit is approached. Epidote is stable at lower temperatures (typically >280 °C; Reyes, 1990), and so the epidote subzone may extend for several kilometers laterally from a large porphyry deposit, depending on the local thermal profile and hydrology (**Figure 1**). At lower temperatures, chlorite, carbonates, and, in mafic volcanic rocks, prehnite and/or zeolites form on the distal fringe of the porphyry deposit, up to 10 km or more from the mineralized center (e.g., Bingham Canyon; Bowman et al., 1987). Mapping of the propylitic subfacies in volcanic terrains (e.g., **Figure 1**) can therefore be an effective vectoring tool. Similar mapping tools need to be developed for porphyry deposits that form in siliciclastic and carbonate wall rocks.

Each of the magmatic and hydrothermal processes that occur in the life cycle of a porphyry system imparts changes to the rock mass, which can be used to explore using standard geological, geochemical, and geophysical exploration techniques. Exploration is more difficult in deformed terranes or buried terranes where the porphyry deposit or district either does not crop out or is barely exposed. These environments host some recent major discoveries such as Resolution and Oyu Tolgoi. In these environments, effective exploration requires a combination of a good geologic model for the terrane, coupled with the intelligent application of geochemistry and geophysics.

Acknowledgments

The authors thank all of their students and colleagues for the lively discussions, insights, and reality checks that they have provided over the years, which have influenced their opinions on the processes required to form porphyry deposits. They also thank Steve Scott for his patience and forbearance as an editor and for his suggestions on how to improve the manuscript. Thanks also to their reviewers, Noel White and Huayong Chen, whose comments also significantly improved the content of this manuscript. PH is grateful for the support from the Natural Sciences and Engineering Research Council that has funded part of this research. DRC thanks the Australian Research Council for their financial support through the Centre of Excellence grant scheme. RMT thanks the U.S. Geological Survey and Natural Sciences and Engineering Research Council for years of support. JW thanks CODES and the Department of Earth Science and Engineering at Imperial College London for providing the opportunity to collaborate on porphyry system research via a Visiting Professor position at CODES.

References

Ahmadian J, Haschke M, McDonald I, et al. (2009) High magmatic flux during Alpine-Himalayan collision: Constraints from the Kal-e-Kafi complex, central Iran. *Geological Society of America Bulletin* 121: 857–868.

Akira I (2000) Mineral paragenesis, fluid inclusions and sulphur isotope systematics of the Lepanto Far South East porphyry Cu–Au deposit, Mankayan, Philippines. *Resource Geology* 50: 151–168.

Alt JC, Shanks WC, and Jackson MC (1993) Cycling of sulfur in subduction zones: The geochemistry of sulfur in the Mariana Island Arc and back-arc trough. *Earth and Planetary Science Letters* 119: 477–494.

Anbar AD (2004) Molybdenum stable isotopes: Observations, interpretations and directions. In: Johnson CM, Beard BL, and Albarède F (eds.) *Geochemistry of Non-traditional Stable Isotopes*. *Reviews in Mineralogy and Geochemistry*, vol. 55, pp. 429–454. Washington, DC: Mineralogical Society of America, Geochemical Society.

Annen C, Blundy JD, and Sparks RSJ (2006) The genesis of intermediate and silicic magmas in deep crustal hot zones. *Journal of Petrology* 47: 505–539.

Arancibia ON and Clark AH (1996) Early magnetite–amphibole–plagioclase alteration-mineralization in the Island copper porphyry copper–gold–molybdenum deposit, British Columbia. *Economic Geology* 91: 402–438.

Arribas A Jr. and Tosdal RM (1994) Isotopic composition of Pb in ore deposits of the Betic Cordillera, Spain: Origin and relationship to other European deposits. *Economic Geology* 89: 1074–1093.

Audétat A, Günther D, and Heinrich CA (1998) Formation of a magmatic–hydrothermal ore deposit: Insights with LA-ICP-MS analysis of fluid inclusions. *Science* 279: 2091–2279.

Audétat A, Pettke T, Heinrich CH, and Bodnar RJ (2008) The composition of magmatic–hydrothermal fluids in barren and mineralized intrusions. *Economic Geology* 103: 877–908.

Bacon CR (1983) Eruptive history of Mount Mazama and Crater Lake Caldera, Cascade Range, USA. *Journal of Volcanology and Geothermal Research* 18: 57–115.

Baker T and Thompson JFH (1998) Fluid evolution at the Red Chris porphyry Cu–Au deposit, Northwest British Columbia. *Geological Society of America Abstracts with Programs* 30: 367.

Ballard JR, Palin JM, Williams IS, Campbell IH, and Faunes A (2001) Two ages of porphyry intrusion resolved for the super-giant Chuquicamata copper deposit of northern Chile by ELA-ICP-MS and SHRIMP. *Geology* 29: 383–386.

Barling J, Arnold GL, and Anbar AD (2001) Natural mass-dependent variations in the isotopic composition of molybdenum. *Earth and Planetary Science Letters* 193: 447–457.

Barnes S and Maier WD (1999) The fractionation of Ni, Cu and the noble metals in silicate and sulfide liquids. Short Course Notes, *Geological Association of Canada* 13: 69–106.

Barra F, Ruiz J, Valencia VA, et al. (2005) Laramide porphyry Cu–Mo mineralization in northern Mexico; age constraints from Re–Os geochronology in molybdenite. *Economic Geology* 100: 1605–1616.

Barreiro BA and Clark AH (1984) Lead isotopic evidence for evolutionary changes in magmacrust interaction, Central Andes, southern Peru. *Earth and Planetary Science Letters* 69: 30–42.

Batchelder J (1977) Light stable isotope and fluid inclusion study of the porphyry copper deposit at Copper Canyon, Nevada. *Economic Geology* 72: 60–70.

Beane RE (1982) Hydrothermal alteration in silicate rocks; southwestern North America. In: Titley SR (ed.) *Advances in Geology of Porphyry Copper Deposits; Southwestern North America*, pp. 117–137. Tucson, AZ: University of Arizona Press.

Beard BL and Johnson CM (2004) Fe isotope variations in the modern and ancient Earth and other planetary bodies. In: Johnson CM, Beard BL, and Albarede F (eds.) *Geochemistry of Non-traditional Stable Isotopes*. *Reviews in Mineralogy and Geochemistry*, vol. 55, pp. 319–358. Washington, DC: Mineralogical Society of America.

Best MG and Christiansen EH (2001) *Igneous Petrology*. Malden, MA: Blackwell Science.

Bissig T, Clark AH, Lee J, and von Quadt A (2003) Petrogenetic and metallogenetic responses to Miocene slab flattening: New constraints from the El Indio-Pascua Au–Ag–Cu belt, Chile/Argentina. *Mineralium Deposita* 38: 844–862.

Bodnar RJ (1995) Fluid-inclusion evidence for a magmatic source for metals in porphyry copper deposits. In: Thompson JFH (ed.) Short Course Handbook, *Magmas, Fluids, and Ore Deposits*, vol. 23, pp. 139–152. Victoria, BC: Mineralogical Association of Canada.

Bodnar RJ, Burnham CW, and Sterner SM (1985) Synthetic fluid inclusions in natural quartz. III. Determination of phase equilibrium properties in the system H_2O–NaCl to 1000 °C and 1500 bars. *Geochimica et Cosmochimica Acta* 49: 1861–1873.

Bouse RM, Ruiz J, Titley SR, Tosdal RM, and Wooden JL (1999) Lead isotope compositions of Late Cretaceous and Early Tertiary igneous rocks and sulfide minerals in Arizona: Implications for the sources of plutons and metals in porphyry copper deposits. *Economic Geology* 94: 211–244.

Bowman JR, Parry WT, Kropp WP, and Kruser SA (1987) Chemical and isotopic evolution of hydrothermal solutions at Bingham, Utah. *Economic Geology* 82: 395–428.

Braxton DP, Cooke DR, Dunlap J, et al. (2012) From crucible to graben in 2.3 Ma: A high-resolution geochronological study of porphyry life cycles, Boyongan-Bayugo copper–gold deposits, Philippines. *Geology* 40: 471–474.

Braxton DP and Mathur R (2011) Exploration applications of copper isotopes in the supergene environment: A case study of the Bayugo porphyry copper–gold deposit, southern Philippines. *Economic Geology* 106: 1447–1463.

Burnham CW (1979) Magmas and hydrothermal fluids. In: Barnes HL (ed.) *Geochemistry of Hydrothermal Ore Deposits*, vol. 2. pp, 71–136. New York, NY: John Wiley and Sons.

Burnham CW (1985) Energy release in subvolcanic environments: Implications for breccia formation. *Economic Geology* 80: 1515–1522.

Burnham CW and Ohmoto H (1980) Late-stage processes of felsic magmatism. *Mining Geology,* Special Issue, 8: 1–11.

Campos E, Wijbrans J, and Andriessen PAM (2009) New thermochronologic constraints on the evolution of the Zaldívar porphyry copper deposit, northern Chile. *Mineralium Deposita* 44: 329–342.

Camus F (2003) *Geología de los sistemas porfíricos en los Andes de Chile*. p, 267. Santiago: Servicio Nacional de Geología y Minería.

Candela PA (1991) Physics of aqueous phase evolution in plutonic environments. *American Mineralogist* 76: 1081–1091.

Cannell J, Cooke DR, Walshe JL, and Stein H (2005) Geology, mineralization, alteration, and structural evolution of the El Teniente porphyry Cu–Mo deposit. *Economic Geology* 100: 979–1003.

Carr GR, Dean JA, Suppel DW, and Heithersay PS (1995) Precise lead isotope fingerprinting of hydrothermal activity associated with Ordovician to Carboniferous metallogenic events in the Lachlan fold belt of New South Wales. *Economic Geology* 90: 1467–1505.

Cathles LM and Shannon R (2007) How potassium silicate alteration suggests the formation of porphyry ore deposits begins with the nearly explosive but barren expulsion of large volumes of magmatic water. *Earth and Planetary Science Letters* 262: 92–108.

Chang Z, Hedenquist J, White N, et al. (2011) Exploration tools for linked porphyry and epithermal deposits; example from the Mankayan intrusion-centered Cu–Au district, Luzon, Philippines. *Economic Geology* 106: 1365–1398.

Chiaradia M and Fontbote L (2002) Lead isotope systematics of Late Cretaceous-Tertiary Andean Arc magmas and associated ores between 8 degrees N and 40 degrees S; evidence for latitudinal mantle heterogeneity beneath the Andes. *Terra Nova* 14: 337–342.

Cline JS and Bodnar RJ (1991) Can economic porphyry copper mineralization be generated by a typical calc-alkaline melt? *Journal of Geophysical Research* 96: 8113–8126.

Cloos M, Sapiie B, Van Ufford AQ, et al. (2005) Collisional delamination in New Guinea – The geotectonics of subducting slab breakoff. Special Paper, *Geological Society of America* 400: 51.

Coira B, Davidson J, Mpodozis C, and Ramos V (1982) Tectonic and magmatic evolution of the Andes of northern Argentina and Chile. *Earth-Science Reviews* 18: 303–332.

Cooke DR and Bloom MS (1990) Epithermal and subjacent porphyry style mineralization, Acupan, Baguio District, Philippines: A fluid inclusion and paragenetic study. *Journal of Geochemical Exploration* 35: 297–340.

Cooke DR, Deyell CL, Waters PJ, Gonzales RI, and Zaw K (2011) Evidence for magmatic–hydrothermal fluids and ore-forming processes in epithermal and porphyry deposits of the Baguio district, Philippines. *Economic Geology* 106: 1399–1424.

Cooke DR, Harris AC, Braxton DP, and Simpson KA (2007) Basins, breccias and basement – Diverse settings for porphyry deposits. In: Andrew CJ, et al. (ed.) *Digging Deeper: Proceedings of the 9th Biennial SGA Meeting Dublin 2007*, pp. 395–398. Dublin, Ireland: Irish Association for Economic Geology.

Cooke DR, Hollings P, and Walshe J (2005) Giant porphyry deposits – Characteristics, distribution and tectonic controls. *Economic Geology* 100: 801–818.

Cooke DR and Simmons SF (2000) Characteristics and genesis of epithermal gold deposits. *Reviews in Economic Geology* 13: 221–244.

Cornejo PC, Tosdal RM, Mpodozis C, et al. (1997) El Salvador, Chile porphyry copper deposit revisited; geologic and geochronologic framework. *International Geology Review* 39: 22–54.

Davidson J, Turner S, Handley H, Macpherson C, and Dosseto A (2007) Amphibole "sponge" in arc crust? *Geology* 35: 787–790. http://dx.doi.org/10.1130/G23637A.1.

Davies JH and von Blankenburg F (1995) Slab breakoff: A model of lithosphere detachment and its test in the magmatism and deformation of collisional orogens. *Earth and Planetary Science Letters* 129: 85–102. http://dx.doi.org/10.1016/0012-821X(94)00237-S.

Deckart K, Clark AH, Aquilar C, and Vargas R (2005) Magmatic and hydrothermal chronology of the supergiant Rio Blanco porphyry copper deposit, central Chile: Implications of an integrated U–Pb and ^{40}Ar–^{39}Ar database. *Economic Geology* 100: 905–934.

Defant M and Kepezhinskas P (2001) Evidence suggests slab melting in arc magmas. *Eos* 82: 65–69.

DePaolo DJ (1981) Trace-element and isotopic effects of combined wallrock assimilation and fractional crystallisation. *Earth and Planetary Science Letters* 53: 189–202.

Deyell CL and Tosdal R (2005) Sulfur isotopic zonation in alkalic porphyry Cu–Au systems II: Application to mineral exploration in British Columbia. *Geological Fieldwork: A Summary of Field Activities and Current Research 2005–1*, pp. 191–208. British Columbia: Ministry of Energy, Mines and Petroleum Resources.

Dilles JH, Einaudi MT, Proffett J, and Barton MD (2000) Overview of the Yerington porphyry copper district – Magmatic to non-magmatic sources of hydrothermal fluids – Their flow paths and alteration effects on rocks and Cu–Mo–Fe–Au ores. *Society of Economic Geologists Guidebook Series* 32: 55–66.

Dilles JH, Martin MW, Stein H, and Rusk B (2003) Re–Os and Up–Pb ages for the Butte copper district, Montana: A short-lived or long-lived hydrothermal system? *Geological Society of America Abstracts with Programs, Paper No. 163–1.*

Dilles JH and Wright JE (1988) The chronology of early Mesozoic arc magmatism in the Yerington district, Nevada, and its regional implications. *Geological Society of America Bulletin* 100: 644–652.

Dreyer BM, Morris JD, and Gill B (2010) Incorporation of subducted slab-derived sediment and fluid in arc magmas: B–Be–^{10}Be-ε_{Nd} systematics of the Kurile Convergent Margin, Russia. *Journal of Petrology* 51: 1761–1782.

Drummond SE and Ohmoto H (1985) Chemical evolution and mineral deposition in boiling hydrothermal systems. *Economic Geology* 80: 126–147.

Eastoe CJ (1978) A fluid inclusion study of the Panguna porphyry copper deposit, Bougainville, Papua New Guinea. *Economic Geology* 73: 721–748.

Eaton PC and Setterfield TN (1993) The relationship between epithermal and porphyry hydrothermal systems within the Tavua Caldera, Fiji. *Economic Geology* 88: 1053–1083.

Ehrlich S, Butler I, Halicza L, et al. (2004) Experimental study of the copper isotope fractionation between aqueous Cu(II) and covellite, CuS. *Chemical Geology* 209: 259–269.

Field CW, Zhang L, Dilles JH, Rye RO, and Reed MH (2005) Sulfur and oxygen isotope record in sulfate and sulfide minerals of early, deep, pre-Main Stage porphyry Cu–Mo and late Main Stage base-metal mineral deposits, Butte district, Montana. *Chemical Geology* 215: 61–93.

Fiorentini M and Garwin S (2010) Evidence of a mantle contribution in the genesis of magmatic rocks from the Neogene Batu Hijau district in the Sunda Arc, South Western Sumbawa, Indonesia. *Contributions to Mineralogy and Petrology* 159: 819–837.

Fournier RO (1999) Hydrothermal processes related to movement of fluid from plastic into brittle rock in the magmatic–epithermal environment. *Economic Geology* 94: 1193–1211.

Frikken P, Cooke DR, Walshe JL, et al. (2005) Mineralogical and isotopic zonation in the Sur-Sur tourmaline breccia, Rio Blanco-Los Bronces Cu–Mo deposit, Chile: Implications for ore genesis. *Economic Geology* 100: 935–961.

Garwin S (2002) The geologic setting of intrusion-related hydrothermal systems near the Batu Hijau porphyry copper–gold deposit, Sumbawa, Indonesia. *Society of Economic Geologists,* Special Publication, 9: 333–366.

Giggenbach WF (1992) Isotopic shifts in waters from geothermal and volcanic systems along convergent plate boundaries and their origin. *Earth and Planetary Science Letters* 113: 495–510.

Gill JB (1981) *Orogenic Andesites and Plate Tectonics*. p. 390. New York, NY: Springer.

Glazner AF, Bartley JM, Coleman DS, Gray W, and Taylor ZT (2004) Are plutons assembled over millions of years by amalgamation from small magma chambers? *GSA Today* 14: 4–11.

Glen RA, Crawford AJ, and Cooke DR (2007) Tectonic setting of porphyry Cu–Au mineralisation in the Ordovician–Early Silurian Macquarie Arc, Eastern Lachlan Orogen, New South Wales. *Australian Journal of Earth Sciences* 54: 465–479.

Glen R, Quinn C, and Cooke DR (2012) The Macquarie Arc, Lachlan Orogen, New South Wales: Its evolution, tectonic setting and mineral deposits. *Episodes* 35: 177–186.

Graham S, Pearson N, Jackson S, Griffin W, and O'Reilly SY (2004) Tracing Cu and Fe from source to porphyry: In situ determination of Cu and Fe isotope ratios in sulfides from the Grasberg Cu–Au deposit. *Chemical Geology* 207: 147–169.

Gustafson LB and Hunt JP (1975) The porphyry copper deposit at El Salvador, Chile. *Economic Geology* 70: 857–912.

Gustafson LB, Orquera W, McWilliams M, et al. (2001) Multiple centers of mineralization in the Indio Muerto District, El Salvador, Chile. *Economic Geology* 96: 325–350.

Hannah J, Stein HJ, Wieser ME, De Laeter JR, and Varner MD (2007) Molybdenum isotope variations in molybdenite; vapor transport and Rayleigh fractionation of Mo. *Geology* 35: 703–706.

Harris AC, Allen CM, Bryan SE, et al. (2004) ELA-ICP-MS U–Pb zircon geochronology of regional volcanism hosting the Bajo de la Alumbrera Cu–Au deposit: Implications for porphyry-related mineralization. *Mineralium Deposita* 39: 46–67.

Harris AC, Bryan SE, and Holcombe RJ (2006) Volcanic setting of the Bajo de la Alumbrera porphyry Cu–Au deposit, Farallon Negro Volcanics, Northwest Argentina. *Economic Geology* 101: 71–94.

Harris AC, Dunlap WJ, Reiners PW, et al. (2008) Multimillion year thermal history of a porphyry copper deposit: Application of U–Pb, $^{40}Ar/^{39}Ar$ and (U–Th)/He chronometers, Bajo de la Alumbrera copper–gold deposit, Argentina. *Mineralium Deposita* 43: 295–314.

Harris AC and Golding SD (2002) New evidence of magmatic-fluid-related phyllic alteration: Implications for the genesis of porphyry Cu deposits. *Geology* 30: 335–338.

Harris AC, Golding SD, and White NC (2005) Bajo de la Alumbrera copper–gold deposit; stable isotope evidence for a porphyry-related hydrothermal system dominated by magmatic aqueous fluids. *Economic Geology* 100: 863–886.

Harris AC, Kamenetsky VS, White NC, van Achterbergh E, and Ryan CG (2003) Melt inclusions in veins: Linking magmas and porphyry Cu deposits. *Science* 302: 2109–2111.

Haschke M, Ahmadian J, Murata M, and McDonald I (2010) Copper mineralization prevented by arc-root delamination during Alpine-Himalayan collision in Central Iran. *Economic Geology* 105: 855–865.

Haschke M, Siebel W, Gunther A, and Scheuber E (2002) Repeated crustal thickening and recycling during the Andean orogeny in north Chile (21°–26°S). *Journal of Geophysical Research* 107(B1): 2019. http://dx.doi.org/10.1029/2001JB000328.

Hattori K and Keith JD (2001) Contribution of mafic melt to porphyry copper mineralization: Evidence from Mount Pinatubo, Philippines, and Bingham Canyon, Utah, USA. *Mineralium Deposita* 36: 799–806.

Hedenquist JW, Arribas A Jr., and Reynolds TJ (1998) Evolution of an intrusion-centred hydrothermal system: Far Southeast-Lepanto Porphyry and Epithermal Cu–Au deposits, Philippines. *Economic Geology* 93: 373–404.

Hedenquist JW and Richards JP (1998) The influence of geochemical techniques on the development of genetic models for porphyry copper deposits. *Reviews in Economic Geology* 10: 235–256.

Heidrick TL and Titley SR (1982) Fracture and dike patterns in Laramide plutons and their structural and tectonic implications: American south-west. In: Titley SR (ed.) *Advances in Geology of the Porphyry Copper Deposits*, pp. 73–91. Tucson, AZ: University of Arizona Press.

Heinrich CA, Driesner T, Stefánsson A, and Seward TM (2004) Magmatic vapor contraction and the transport of gold from the porphyry environment to epithermal ore deposits. *Geology* 32: 761–764.

Heinrich CA, Günter D, Audétat A, Ulrich T, and Frischknecht R (1999) Metal fractionation between magmatic brine and vapor determined by microanalysis of fluid inclusions. *Geology* 27: 755–758.

Heinrich CA, Ryan CG, Mernagh TP, and Eadington PJ (1992) Segregation of ore metals between magmatic brine and vapor – A fluid inclusion study using PIXE microanalysis. *Economic Geology* 87: 23–43.

Heithersay PS and Walshe JL (1995) Endeavour 26 North: A porphyry copper–gold deposit in the Late Ordovician shoshonitic Goonumbla Volcanic Complex, New South Wales, Australia. *Economic Geology* 90: 1506–1532.

Henley RW and McNabb A (1978) Magmatic vapor plumes and ground-water interaction in porphyry copper emplacement. *Economic Geology* 73: 1–20.

Hildreth W and Moorbath S (1988) Crustal contribution to arc magmatism in the Andes of Central Chile. *Contributions to Mineralogy and Petrology* 98: 455–489.

Hoefs J (2009) *Stable Isotope Geochemistry*, vol. 6, p. 285. Berlin: Springer.

Holliday JR and Cooke DR (2007) Advances in geological models and exploration methods for copper + or − gold porphyry deposits. *Proceedings – Decennial International Conference on Mineral Exploration* 5, pp. 791–809. Toronto, Canada.

Holliday JR, Wilson A, Blevin P, et al. (2002) Porphyry gold–copper mineralization in the Cadia district, eastern Lachlan Fold Belt, New South Wales, and its relationship to shoshonitic magmatism. *Mineralium Deposita* 37: 100–116.

Hollings P, Cooke DR, and Clark A (2005) Regional geochemistry of Tertiary volcanic rocks in Central Chile: Implications for tectonic setting and ore deposit genesis. *Economic Geology* 100: 887–904.

Hollings P, Cooke DR, Waters P, and Cousens B (2011a) Igneous geochemistry of mineralized rocks of the Baguio District, Philippines: Implications for tectonic evolution and the genesis of porphyry-style mineralisation. *Economic Geology* 106: 1317–1333.

Hollings P, Wolfe R, Cooke DR, and Waters P (2011b) Geochemistry of tertiary igneous rocks of Northern Luzon, Philippines: Evidence for a back arc-setting for alkalic porphyry copper–gold deposits and a case for slab roll-back? *Economic Geology* 106: 1257–1277.

Hou ZQ and Cook NJ (2009) Metallogenesis of the Tibetan collisional orogen: A review and introduction to the special issue. *Ore Geology Reviews* 36: 2–24.

Hou Z, Yang Z, Qu X, et al. (2009) The Miocene Gangdese porphyry copper belt generated during post-collisional extension in the Tibetan Orogen. *Ore Geology Reviews* 36: 25–51.

Imai A (2001) Generation and evolution of ore fluids for porphyry Cu–Au mineralization of the Santo Tomas II (Philex) deposit, Philippines. *Resource Geology* 51: 71–96.

Jensen EP and Barton MD (2000) Gold deposits related to alkaline magmatism. *Reviews in Economic Geology* 13: 279–314.

Jiang Y-H, Jiang S-Y, Ling HF, and Dai B-Z (2006) Low-degree melting of a metasomatized lithospheric mantle for the origin of Cenozoic Yulong monzogranite-porphyry, east Tibet: Geochemical and Sr–Nd–Pb–Hf isotopic constraints. *Earth and Planetary Science Letters* 241: 617–633. http://dx.doi.org/10.1016/j.epsl.2005.11.023.

Johnson CM, Beard BL, and Albarede F (eds.) (2004) *Geochemistry of Non-traditional Stable Isotopes*. In: *Reviews in Mineralogy and Geochemistry* 55. Washington, DC: Mineralogical Society of America.

Jones PR III (1981) Crustal structures of the Peru continental margin and adjacent Nazca Plate 9°S latitude. *Geological Society of America Memoirs* 86: 423–443.

Jugo PJ (2009) Sulfur content at sulfide saturation in oxidized magmas. *Geology* 37: 415–418.

Kamenov G, Macfarlane AW, and Riciputi L (2002) Sources of lead in the San Cristobal, Pulacayo, and Potosi mining districts, Bolivia, and a reevaluation of regional ore lead isotope provinces. *Economic Geology* 97: 573–592.

Kay SM and Kurtz A (1995) Magmatic and tectonic characterization of the El Teniente region. *Internal Report*, *El Teniente Division*, *CODELCO-Chile*, 180p.

Kay SM, Mpodozis C, and Coira B (1999) Neogene magmatism, tectonism and mineral deposits of the central Andes. *Society of Economic Geologists* Special Publication, 7: 27–59.

Keith JD, Whitney JA, Hattori K, et al. (1997) The role of magmatic sulfides and mafic alkaline magmas in the Bingham and Tintic mining districts, Utah. *Journal of Petrology* 38: 1679–1690.

Kerrich R, Goldfarb R, Groves D, Garwin S, and Jia Y (2000) The characteristics, origins, and geodynamic settings of supergiant gold metallogenic provinces. *Science in China Series D (Earth Sciences)* 43: 1–68.

Kesler SE (1973) Copper, molybdenum and gold abundances in porphyry copper deposits. *Economic Geology* 68: 106–112.

Khashgerel B-E, Rye RO, Hedenquist JW, and Kavalieris I (2006) Geology and reconnaissance stable isotope study of the Oyu Tolgoi porphyry copper–Au system, South Gobi, Mongolia. *Economic Geology* 101: 503–522.

Klemm LM, Pettke T, Heinrich CA, and Campos E (2007) Hydrothermal evolution of the El Teniente Deposit, Chile; porphyry Cu–Mo ore deposition from low-salinity magmatic fluids. *Economic Geology* 102: 1021–1045.

Kouzmanov K, Moritz R, von Quadt A, et al. (2009) Late Cretaceous porphyry Cu and epithermal Cu–Au association in the southern Panagyurishte District, Bulgaria; the paired Vlaykov Vruh and Elshitsa deposits. *Mineralium Deposita* 44: 611–646.

Kusakabe M, Hori M, and Yukihhiro M (1990) Primary mineralization-alteration of the El Teniente and Río Blanco porphyry copper deposits, Chile: Stable isotopes, fluid inclusions and $Mg^{2+}/Fe^{2+}/Fe^{3+}$ ratios in hydrothermal biotite. *University of Western Australia Publication* 2: 244–259.

Kusakabe M, Nakagawa S, Hori M, et al. (1984) Oxygen and sulphur isotopic compositions of quartz, anhydrite, and sulfide minerals from the El Teniente and Río Blanco porphyry copper deposits, Chile. *Bulletin of the Geological Survey of Japan* 35: 583–614.

Landtwing MR, Furrer C, Redmond PB, et al. (2010) The Bingham Canyon porphyry Cu–Mo–Au deposit. III. Zoned copper–gold ore deposition by magmatic vapor expansion. *Economic Geology* 105: 91–118.

Lang JR, Stanley CR, Thompson JFH, and Dunne KPE (1995) Na–K–Ca magmatic–hydrothermal alteration in alkalic porphyry Cu–Au deposits, British Columbia. *Mineralogical Association of Canada Short Course* 23: 339–366.

Larson PB, Maher K, Ramos FC, et al. (2003) Copper isotope ratios in magmatic and hydrothermal ore-forming environments. *Chemical Geology* 201: 337–350.
Leeman WP (1996) Boron and other fluid-mobile elements in volcanic arc lavas: Implications for subduction processes. In: Bebout GE, Scholl DW, Kirby SH, and Platt JP (eds.) *Subduction: Top to Bottom*, pp. 269–276. Washington, DC: American Geophysical Union.
Li W, Jackson SE, Pearson NJ, and Graham S (2010) Copper isotopic zonation in the Northparkes porphyry Cu–Au deposit, SE Australia. *Geochimica et Cosmochimica Acta* 74: 4078–4096.
Lickfold V (2002) *Intrusive History and Volatile Evolution of the Endeavour Porphyry Cu–Au Deposits, Goonumbla District, NSW, Australia*. Unpublished PhD Thesis, University of Tasmania, Hobart, Australia, 230 p.
Lickfold V, Cooke DR, Crawford AJ, and Fanning C (2007) Shoshonitic magmatism and the formation of the Northparkes porphyry Cu–Au deposits, New South Wales. *Australian Journal of Earth Sciences* 54: 417–444.
Lickfold V, Cooke DR, Smith SG, and Ullrich TD (2003) Endeavour copper–gold porphyry deposits, Northparkes, New South Wales – Intrusive history and fluid evolution. *Economic Geology* 98: 1607–1636.
Lindsay DD, Zentilli M, and Rojas de la Rivera J (1995) Evolution of an active ductile to brittle shear system controlling mineralization at the Chuquicamata porphyry copper deposit, northern Chile. *International Geology Review* 37: 945–958.
Loucks R (2012) Chemical characteristics, geodynamic setting and petrogenesis of copper-ore-forming arc magmas. *Centre for Exploration Targeting Quarterly Newsletter* 19: 1–10.
Lowell JD and Guilbert JM (1970) Lateral and vertical alteration-mineralization zoning in porphyry ore deposits. *Economic Geology* 65: 373–408.
Macfarlane AW, Marcet P, LeHuray AP, and Petersen U (1990) Lead isotope provinces of Central Andes inferred from ores and crustal rocks. *Economic Geology* 85: 1857–1880.
Maher KC, Jackson S, and Mountain B (2011) Experimental evaluation of the fluid-mineral fractionation of Cu isotopes at 250 °C and 300 °C. *Chemical Geology* 286: 229–239.
Maksaev V, Munizaga F, McWilliams M, et al. (2004) New chronology for El Teniente, Chilean Andes, from U/Pb, $^{40}Ar/^{39}Ar$, Re/Os, and fission-track dating; implications for the evolution of a supergiant porphyry Cu-Mo deposit. In: Sillitoe RH, Perello J, and Vidal CE (eds.) Special Publication, vol. 11, Littleton, CO: Society of Economic Geologists.
Manning CE (2004) The chemistry of subduction-zone fluids. *Earth and Planetary Science Letters* 223: 1–16.
Massonne H-J (1992) Evidence for low-temperature ultrapotassic siliceous fluids in subduction zone environments from experiments in the system K_2O–MgO–Al_2O_3–SiO_2–H_2O (KMASH). *Lithos* 28: 421–434.
Masterman GJ, Cooke DR, Berry RF, et al. (2004) Magmatic, alteration and mineralisation history of copper–molybdenum porphyry deposits and related copper–silver high sulfidation epithermal mineralisation in the Collahuasi district, northern Chile. *Economic Geology* 99: 673–690.
Masterman GJ, Cooke DR, Berry RF, et al. (2005) Fluid chemistry, structural setting, and emplacement history of the Rosario Cu–Mo porphyry and Cu–Ag–Au epithermal veins, Collahuasi district, northern Chile. *Economic Geology* 100: 835–862.
Mathur R, Brantley S, Anbar A, et al. (2010) Variation of Mo isotopes from molybdenite in high-temperature hydrothermal ore deposits. *Mineralium Deposita* 45: 43–50.
Mathur R, Ruiz J, Titley S, et al. (2005) Cu isotopic fractionation in the supergene environment with and without bacteria. *Geochimica et Cosmochimica Acta* 69: 5233–5246.
Mathur R, Titley S, Barra F, et al. (2009) Exploration potential of Cu isotope fractionation in porphyry copper deposits. *Journal of Geochemical Exploration* 102: 1–6.
McInnes BIA, McBride JS, Evans NJ, Lambert DD, and Andrew AS (1999) Osmium isotope constraints on ore metal recycling in subduction zones. *Science* 286: 512–516.
McManus J, Nägler TF, Siebert S, Wheat CG, and Hammond DE (2002) Oceanic molybdenum isotope fractionation: Diagenesis and hydrothermal ridge-flank alteration. *Geochemistry, Geophysics, Geosystems* 3: 1078. http://dx.doi.org/10.1029/2002GC000356.
Meyer C and Hemley JJ (1967) Wall rock alteration. In: Barnes HL (ed.) *Geochemistry of Hydrothermal Ore Deposits*, pp. 166–235. New York, NY: Holt, Rinehart, and Winston.
Müller D and Groves DI (2000) *Potassic Igneous Rocks and Associated Gold–Copper Mineralization*, p. 238. Berlin: Springer.
Müller D, Heithersay PS, and Groves DI (1994) The shoshonite porphyry Cu–Au association in the Goonumbla district, N.S.W., Australia. *Mineralogy and Petrology* 51: 299–321.
Müller D, Kaminski K, Uhlig S, et al. (2002) The transition from porphyry- to epithermal-style gold mineralization at Ladolam, Lihir Island, Papua New Guinea: A reconnaissance study. *Mineralium Deposita* 37: 61–74.
Mungall JE (2002) Roasting the mantle: Slab melting and the genesis of major Au and Au-rich Cu deposits. *Geology* 30: 915–918.
Nash JT (1976) Fluid inclusion petrology; data from porphyry copper deposits and applications to exploration. Professional Paper, *U.S. Geological Survey* 907D: 16.
Ohmoto H (1986) Stable isotope geochemistry of ore deposits. In: Valley JW, Taylor HP Jr., and O'Neil JR (eds.) *Stable Isotopes in High Temperature Geological Processes. Reviews in Mineralogy*, vol. 16, pp. 491–559. Washington, DC: Mineralogical Society of America.
Ohmoto H and Rye RO (1979) Isotopes of sulfur and carbon. In: Barnes HL (ed.) *Geochemistry of Hydrothermal Ore Deposits*, vol. 2, pp. 509–567. New York, NY: Wiley.
Ossandon CG, Freraut CR, Gustafson LB, Lindsay DD, and Zentilli M (2001) Geology of the Chuqicamata Mine; a progress report. *Economic Geology* 96: 249–270.
Padilla-Garza RA, Titley SR, and Eastoe CJ (2004) Hypogene evolution of the Escondida porphyry copper deposit, Chile. In: Sillitoe RH, Perello J, and Vidal CE (eds.) *Andean Metallogeny: New Discoveries, Concepts, and Updates*, Special Publication, vol. 11, Littleton, CO: Society of Economic Geologists.
Pass HE, Cooke DR, Davidson G, et al. (in press) Alteration and isotope geochemistry of the Northeast Zone, Mt. Polley alkalic Cu–Au porphyry deposit, British Columbia: A case for carbonate assimilation? *Economic Geology*.
Perello J, Carlotto V, Zarate A, et al. (2003) Porphyry-style alteration and mineralization of the middle Eocene to early Oligocene Andahuaylas-Yauri Belt, Cuzco region, Peru. *Economic Geology* 98: 1575–1605.
Petke T, Oberli F, and Heinrich C (2010) The magma and metal source of giant porphyry-type ore deposits, based on lead isotope microanalysis of individual fluid inclusions. *Earth and Planetary Science Letters* 296: 267–277.
Pietruszka AJ, Walker RJ, and Candela PA (2006) Determination of mass-dependent molybdenum isotopic variations by MC-ICP-MS: An evaluation of matrix effects. *Chemical Geology* 225: 121–136.
Pokrovski GS, Borisova AY, and Harrichoury J-C (2008) The effect of sulfur on vapour–liquid fractionation of metals in hydrothermal systems. *Earth and Planetary Science Letters* 266: 345–362.
Polve M, Maury RC, Jego S, et al. (2007) Temporal geochemical evolution of Neogene magmatism in the Baguio gold–copper mining district (Northern Luzon, Philippines). *Resource Geology* 57: 197–218.
Pudack C, Halter WE, Heinrich CA, and Pettke T (2009) Evolution of magmatic vapor to gold-rich epithermal liquid: The porphyry to epithermal transition at Nevados de Famatina, northwest Argentina. *Economic Geology* 104: 449–477.
Redmond PB and Einaudi MT (2010) The Bingham Canyon porphyry Cu–Mo–Au deposit. I. Sequence of intrusions, vein formation, and sulfide deposition. *Economic Geology* 105: 43–68.
Redmond PB, Einaudi MT, Inan EE, Landtwing MR, and Heinrich CA (2004) Copper deposition by fluid cooling in intrusion-centered systems – New insights from the Bingham porphyry ore deposit, Utah. *Geology* 32: 217–220.
Reich M, Parada MA, Palacios C, et al. (2003) Adakite-like signature of late Miocene intrusions at the Los Pelambres giant porphyry copper deposit in the Andes of Central Chile: Metallogenic implications. *Mineralium Deposita* 38: 876–885.
Reyes AG (1990) Petrology of Philippine geothermal systems and the application of alteration mineralogy to their assessment. *Journal of Volcanology and Geothermal Research* 43: 279–309.
Reynolds TJ and Beane RE (1985) Evolution of hydrothermal fluid characteristics at the Santa Rita, New Mexico, porphyry copper deposit. *Economic Geology* 80: 1328–1347.
Richards JP (1995) Alkalic-type epithermal gold deposits, a review. In: Thompson JFH (ed.) *Magmas, Fluids, and Ore Deposits. Mineralogical Association of Canada Short Course*, vol. 23, pp. 367–400. Victoria, BC: Mineralogical Association of Canada.
Richards JP (2003) Tectono-magmatic precursors for porphyry Cu–(Mo–Au) deposit formation. *Economic Geology* 98: 1515–1533.
Richards JP (2009) Postsubduction porphyry Cu–Au and epithermal Au deposits: Products of remelting of subduction-modified lithosphere. *Geology* 37: 247–250.
Richards JP (2011a) Magmatic to hydrothermal metal fluxes in convergent and collided margins. *Ore Geology Reviews* 40: 1–26.
Richards JP (2011b) High Sr/Y arc magmas and porphyry Cu ± Mo ± Au deposits. *Economic Geology* 106: 1075–1081.
Richards JP, Boyce AJ, and Pringle MS (2001) Geological evolution of the Escondida area, northern Chile: A model for spatial and temporal localization of porphyry Cu mineralization. *Economic Geology* 96: 271–305.
Richards JP, Chappell BW, and McCulloch MT (1990) Intraplate-type magmatism in a continent–island-arc collision zone: Porgera intrusive complex, Papua New Guinea. *Geology* 18: 958–961.

Richards JP and Kerrich R (2007) Adakite-like rocks: Their diverse origins and questionable role in metallogenesis. *Economic Geology* 102: 537–576.

Roedder E (1971) Fluid inclusion studies on the porphyry-type ore deposits at Bingham, Utah, Butte, Montana, and Climax, Colorado. *Economic Geology* 66: 98–118.

Roedder E (1984) Fluid inclusions. *Reviews in Mineralogy* 12: 644.

Rose AW and Burt DM (1979) Hydrothermal alteration. In: Barnes HL (ed.) *Geochemistry of Hydrothermal Ore Deposits*, pp. 173–235. New York, NY: Wiley.

Rusk BG, Reed MH, and Dilles JH (2008) Fluid inclusion evidence for magmatic–hydrothermal fluid evolution in the porphyry copper–molybdenum deposit at Butte, Montana. *Economic Geology* 103: 307–334.

Rye RO (1993) The evolution of magmatic fluids in the epithermal environment: The stable isotope perspective. *Economic Geology* 88: 733–752.

Rye RO (2005) A review of the stable isotope geochemistry of sulfate minerals in selected igneous environments and related hydrothermal systems. *Chemical Geology* 215: 5–36.

Rye RO, Bethke PM, and Wasserman MD (1992) The stable isotope geochemistry of acid sulfate alteration. *Economic Geology* 87: 225–262.

Sajona F and Maury R (1998) Association of adakites with gold and copper mineralization in the Philippines. *Comptes Rendus Academy Science Paris, Sciences de la Terre et des Planetes* 326: 27–34.

Sasaki A, Ulriksen CE, Sato K, and Ishihara S (1984) Sulphur isotope reconnaissance of porphyry copper and manto-type deposits in Chile and the Philippines. *Bulletin of the Geological Survey of Japan* 35: 615–622.

Seedorff E, Dilles JH, Proffett JM Jr., et al. (2005) Porphyry deposits – Characteristics and origin of hypogene features. *Society of Economic Geologists, Economic Geology* 100th Anniversary Volume, 1905–2005, 251–298.

Seo JH, Guillong M, and Heinrich CA (2012) Separation of molybdenum and copper in porphyry deposits: The roles of sulfur, redox, and pH in ore mineral deposition at Bingham Canyon. *Economic Geology* 243: 333–356.

Seo JH, Lee SK, and Lee I (2007) Quantum chemical calculations of equilibrium copper (I) isotope fractionations in ore-forming fluids. *Chemical Geology* 107: 225–237.

Shafiei B (2010) Lead isotope signatures of the igneous rocks and porphyry copper deposits from the Krman Cenozoic magmatic arc (SE Iran), and their magmatic-metallogenic implications. *Ore Geology Reviews* 38: 27–36.

Shafiei B, Haschke M, and Shahabpour J (2009) Recycling of orogenic arc crust triggers porphyry Cu mineralization in Kerman Cenozoic arc rocks, southeastern Iran. *Mineralium Deposita* 44: 265–283.

Sheets RW, Nesbitt B, and Muehlenbachs K (1996) Meteoric water component in magmatic fluids from porphyry copper mineralization, Babine Lake area, British Columbia. *Geology* 24: 1091–1094.

Sheppard SMF, Nielsen RL, and Taylor HP Jr. (1969) Oxygen and hydrogen isotope ratios of clay minerals from porphyry copper deposits. *Economic Geology* 64: 755–777.

Sheppard SMF, Nielsen RL, and Taylor HP Jr. (1971) Hydrogen and oxygen isotope ratios in minerals from porphyry copper deposits. *Economic Geology* 66: 515–542.

Shields WR, Murphy TJ, and Garner EL (1964) Absolute isotopic abundance ratio and the atomic weight of a reference sample of copper. *Journal of Research of the National Bureau of Standards* 68A: 589–592.

Shmulovich KI, Landwehr D, Simon K, and Heinrich W (1999) Stable isotope fractionation between liquid and vapor in water–salt systems up to 600 °C. *Chemical Geology* 157: 343–354.

Sillitoe RH (1985) Ore-related breccias in volcanoplutonic arcs. *Economic Geology* 80: 1467–1514.

Sillitoe RH (1988) Epochs of intrusion-related copper mineralisation in the Andes. *Journal of South American Earth Sciences* 1: 89–108.

Sillitoe RH (1995) Exploration of porphyry copper lithocaps: Pacific Rim Congress, Auckland, 1995. *Proceedings: Melbourne, Australasian Institute of Mining and Metallurgy Publication Series* 9/95, pp. 527–532. Auckland, New Zealand.

Sillitoe RH (1997) Characteristics and controls of the largest porphyry copper–gold and epithermal gold deposits in the circum-Pacific region. *Australian Journal of Earth Sciences* 44: 373–388.

Sillitoe RH (2000) Styles of high-sulphidation gold, silver, and copper mineralization in porphyry and epithermal environments. *The AusIMM Proceedings* 305: 19–34.

Sillitoe RH (2002) Some metallogenic features of gold and copper deposits related to alkaline rocks and consequences for exploration. *Mineralium Deposits* 37: 4–13.

Sillitoe RH (2010) Porphyry-copper systems. *Economic Geology* 105: 3–41.

Sillitoe RH and Gappe IM (1984) Philippine porphyry copper deposits: Geologic setting and characteristics. *CCOP Technical Publication* 14: 89.

Sillitoe RH and Mortensen JK (2010) Longevity of porphyry copper formation at Quellaveco, Peru. *Economic Geology* 105: 1157–1162.

Singer DA (1995) World class base and precious metal deposits; a quantitative analysis. *Economic Geology* 90: 88–104.

Skewes A and Stern CR (1994) Tectonic trigger for the formation of late Miocene Cu-rich breccia pipes in the Andes of central Chile. *Geology* 22: 551–554.

Skewes A and Stern CR (1995) Genesis of the giant late Miocene to Pliocene copper deposits of central Chile in the context of Andean magmatic and tectonic evolution. *International Geology Review* 37: 893–909.

Skewes A and Stern CR (1996) Late Miocene mineralized breccias in the Andes of central Chile: Sr and Nd isotopic evidence for multiple magmatic sources. *Society of Economic Geologists,* Special Publication, 5: 33–42.

Solomon M (1990) Subduction, arc reversal, and the origin of porphyry copper–gold deposits in island arcs. *Geology* 18: 630–633.

Sparks RSJ and Marshall LA (1986) Thermal and mechanical constraints on mixing between mafic and silicic magmas. *Journal of Volcanology and Geothermal Research* 29: 99–124.

Stacey JS and Kramers JD (1975) Approximation of terrestrial lead isotope evolution by a two-stage model. *Earth and Planetary Science Letters* 26: 207–221.

Taylor HP Jr. (1974) The application of oxygen and hydrogen isotope studies to problems of hydrothermal alteration and ore deposition. *Economic Geology* 69: 843–883.

Taylor BE (1987) Stable isotope geochemistry of low temperature fluids. *Mineralogical Association of Canada* 13: 337–445.

Taylor BE (1992) In: Hedenquist JW (ed.) *Degassing of H_2O from Rhyolite Magma During Eruption and Shallow Intrusion, and the Isotopic Composition of magmatic water in hydrothermal systems. Magmatic Contributions to Hydrothermal Systems*, vol. 279, pp. 190–194. Japan: Geological Survey of Japan Report.

Taylor HP Jr. (1997) Oxygen and hydrogen isotope relationships in hydrothermal mineral deposits. In: Barnes HL (ed.) *Geochemistry of Hydrothermal Ore Deposits*, vol. 3, pp. 229–302. New York, NY: Wiley.

Thiéblemont D, Stein G, and Lescuyer J (1997) Gisements épithermaux et porphyriques: la connexion adakite. *Comptes Rendus Academy Science Paris, Sciences de la terre et des Planetes* 325: 103–109.

Thompson JFH, Gale VG, Tosdal RM, and Wright WA (2004) Characteristics and formation of the Jeronimo carbonate-replacement gold deposit, Potrerillos district, Chile. In: Sillitoe RH, Perello J, and Vidal CE (eds.) *Andean Metallogeny: New Discoveries, Concepts, and Updates*, Special Publication vol. 11, Littleton, CO: Society of Economic Geologists.

Titley SR (1982) The style and progress of mineralization and alteration in porphyry copper systems: American Southwest. In: Titley SR (ed.) *Advances in Geology of the Porphyry Copper Deposits. Southwestern North America*, pp. 139–184. Tucson, AZ: University of Arizona Press.

Titley SR (2001) Crustal affinities of metallogenesis in the American Southwest. *Economic Geology* 96: 1323–1342.

Tosdal RM and Munizaga F (2003) Lead sources in Mesozoic and Cenozoic Andean ore deposits, north-central Chile (30–34S). *Mineralium Deposita* 38: 234–250.

Tosdal RM, Wooden JL, and Bouse RM (1999) Pb isotopes, ore deposits, and metallogenic terranes. *Society of Economic Geologists, Reviews in Economic Geology* 12: 1–12.

Tossell JA (2005) Calculating the partitioning of the isotopes of Mo between oxidic and sulfidic species in aqueous solution. *Geochimica et Cosmochimica Acta* 69: 2981–2993.

Ulrich T, Günther D, and Heinrich CA (1999) Gold concentrations of magmatic brines and the metal budget of porphyry copper deposits. *Nature* 399: 676–679.

Ulrich T, Günther D, and Heinrich CA (2002) The evolution of a porphyry Cu–Au deposit, based on LA-ICP-MS analysis of fluid inclusions: Bajo de la Alumbrera, Argentina. *Economic Geology* 97: 1889–1920.

Vikre PG (2010) Stable isotope compositions of fluids. In: John DA, Ayuso RA, Barton MD, et al. (eds.) *Porphyry Copper Deposit Model. U. S. Geological Survey Scientific Investigations Report 2010–5070–B*, pp. 87–88

von Quadt A, Erni M, Martinek K, et al. (2011) Zircon crystallization and the lifetimes of ore-forming magmatic–hydrothermal systems. *Geology* 39: 731–734.

von Quadt A, Peytcheva I, Kamenov B, et al. (2002) The Elatsite porphyry copper deposit in the Panagyurishte ore district, Srednogorie, Bulgaria – U–Pb zircon geochronology and isotope-geochemical investigations of magmatism and ore genesis. In: Blundell DJ, Neubauer F, and von Quadt A (eds.) *The Timing and Location of Major Ore Deposits in an Evolving Orogeny*, Special Publications, vol. 204, pp. 119–135. London: Geological Society of London.

Vry VH, Wilkinson JJ, Seguel J, and Millan J (2010) Multistage intrusion, brecciation, and veining at El Teniente, Chile: Evolution of a nested porphyry system. *Economic Geology* 105: 119–153.

Wang Q, Wyman DA, Xu J, et al. (2007) Partial melting of thickened or delaminated lower crust in the middle of eastern China; implications for Cu–Au mineralization. *Journal of Geology* 115: 149–161.

Watanabe Y and Hedenquist JW (2001) Mineralogic and stable isotope zonation at the surface over the El Salvador porphyry copper deposit, Chile. *Economic Geology* 96: 1775–1797.

Waters PJ, Cooke DR, Gonzales RI, and Phillips D (2011) Porphyry and epithermal deposits and $^{40}Ar/^{39}Ar$ geochronology of the Baguio district, Philippines. *Economic Geology* 106: 1335–1363.

Wieser ME and de Laeter JR (2003) A preliminary study of isotope fractionation in molybdenites. *International Journal of Mass Spectrometry* 225: 177–183.

William-Jones AE and Heinrich CA (2005) Vapor transport of metals and the formation of magmatic-hydrothermal ore deposits. *Economic Geology* 105: 1287–1312.

Wilkinson JJ, Wilkinson CC, Vry VH, et al. (2008) Ore fluid chemistry in super-giant porphyry copper deposits. *Proceedings of the PACRIM 2008 Congress*, pp. 295–298. *Gold Coast*, *Australia*. Carlton, Victoria: Australian Institute of Mining and Metallurgy.

Wilson AJ, Cooke DR, and Harper BR (2003) The Ridgeway gold–copper deposit: A high-grade alkalic porphyry deposit in the Lachlan fold belt, New South Wales, Australia. *Economic Geology* 98: 1637–1666.

Wilson AJ, Cooke DR, Harper BJ, and Deyell CL (2007a) Sulfur isotopic zonation in the Cadia district, southeastern Australia – Exploration significance and implication for the genesis of alkalic porphyry gold–copper deposits. *Mineralium Deposita* 42: 465–487.

Wilson AJ, Cooke DR, Stein HJ, et al. (2007b) U–Pb and Re–Os geochronologic evidence for two alkali porphyry ore-forming events in the Cadia district, New South Wales, Australia. *Economic Geology* 102: 3–26.

Wilson CJN and Hildreth W (1997) The Bishop Tuff: New insights and implications from eruptive stratigraphy. *Journal of Geology* 105: 407–439.

Wolfe R and Cooke DR (2011) Geology of the Didipio region and genesis of the Dinkidi alkalic porphyry Cu–Au deposit and related pegmatites, northern Luzon, Philippines. *Economic Geology* 106: 1279–1315.

Wolfe RC, Cooke DR, Hooper B, and Heithersay PS (1996) A magmatic origin for late-stage sericite–alunite alteration at the Endeavour 48 Cu–Au porphyry deposit, Goonumbla, NSW. *Geological Society of Australia Abstracts* 41: 480.

Wooden JL, Stacey JS, Howard KA, Doe BR, and Miller DM (1988) Lead isotopic evidence for the formation of Proterozoic crust in the southwestern United States. In: Ernst WG (ed.) *Metamorphism and Crustal Evolution, Western Conterminous United States, Rubey*, vol. 7, pp. 68–86. Engelwood Cliffs, NJ: Prentice-Hall.

Yang TF, Lee T, Chen CH, et al. (1996) A double island arc between Taiwan and Luzon: Consequence of ridge subduction. *Tectonophysics* 258: 85–101.

Zarasvandi A, Liaghat S, and Zentilli M (2005) Geology of the Darreh-Zerreshk and Ali-Abad porphyry copper deposit, central Iran. *International Geology Review* 47: 620–646.

Zartman RE and Doe BR (1981) Plumbotectonics – The model. *Tectonophysics* 75: 135–162.

Zimmerman A, Stein HJ, Hannah JL, et al. (2008) Tectonic configuration of the Apuseni-Banat-Timok-Srednagorie belt, Balkans-South Carpathians, constrained by high precision Re–Os molybdenite ages. *Mineralium Deposita* 43: 1–21.